Noise Characteristics of the Fiber Ring Lasers

by

Charles Xiao Yu

Submitted to the Department of Electrical Engineering and Computer Science in partial fulfillment of the requirements for the degree of

Master of Engineering

at the

MASSACHUSETTS INSTITUTE OF TECHNOLOGY

April 1, 1996

Author .....
Department of Electrical Engineering and Computer Science
March 15, 1996

Certified by .....
Hermann A. Haus
Institute Professor
Thesis Supervisor

Accepted by .....
Frederic R. Morgenthaler.
Chairman, Departmental Committee on Graduate Students

Noise Characteristics of the Fiber Ring Lasers

by

Charles Xiao Yu

Submitted to the Department of Electrical Engineering and Computer Science on April 1, 1996, in partial fulfillment of the requirements for the degree of Master of Engineering in Electrical Engineering and Computer Science

Abstract

This thesis reports the noise characteristics of the fiber ring lasers, and in particular, those of the modelocked erbium-doped fiber ring lasers operating under additive pulse modelocking(APM) principle. The noise characteristics of the APM lasers operating in the soliton regime and in the non-soliton regime are studied both theoretically and experimentally. For the non-soliton regime the noise of a stretched pulse laser is investigated. We find that the experimental results agree with the theoretical predictions. We also find that the timing jitter of the soliton laser is limited by the quantum noise.

Thesis Supervisor: Hermann A. Haus
Title: Institute Professor

Acknowledgments

I want to thank Prof. Hermann Haus for giving me a place to go after my undergraduate education. I also want to thank him for his guidance, and his neat theories. Re-deriving his equations, I realize that the world is not as simply and logical as I thought. Thinking about his theories, I find that they are not as chaotic as they seem. The world might still be an organized place after all.

I want to thank Dr. Shu Namiki for all his help and his teachings. The work reported in this thesis is done with him. Shu has remarkable patience indeed: he waited for me while I kept telling him that I am too busy, first with the PWE, now with my thesis, to do any research. Shu taught me how to make fiber lasers. Only through playing with these lasers did I realize that Prof. Haus' neat theories really work, not only qualitatively, but qualitatively as well.

I want to thank Farzana Khatri. She is my first UROP supervisor in the ultrafast optics group, and the very best. She is a very kind and caring person, which is rare at MIT. I also want to thank Jalal for all our philosophical discussions. I proved to him that I have two hands!

Finally, I want to thank my family, friends, ex-mentors and colleagues for all their help and encouragement. I want to thank MIT for giving me a great education, and Hewlett-Packard Laboratories for making my internships there enjoyable.

Contents

List of Figures

List of Tables

Chapter 1

Introduction

1.1 Modelocked Lasers

Conceptually, a laser cavity consists of a pair of mirrors which encloses a gain medium. The lasing frequencies are determined by the gain medium and the resonator. Different transverse modes exist in the laser cavity. Each of these modes has an infinite set of eigen-frequencies or longitudinal modes whose frequency spacing is determined by the optical length of the cavity. The fiber lasers in this thesis are constructed using single mode fiber so that only the fundamental transverse mode survives. To generate ultra-short laser pulses, one can simply insert a shutter inside the laser cavity. As shown in Figure 1-1, the shutter opens for the desired interval, and remains closed for the rest of the cavity round trip time[1]. In the frequency domain, the function of such a shutter is to force fixed phase and amplitude relationships between different longitudinal modes. The laser output will be a well-defined periodic function in time, and is considered to be "modelocked". Mode-locking leads to a broadened spectrum, or a short pulse.

An approximation to the shutter mentioned above is an intracavity amplitude or phase modulator. If driven at the cavity round trip frequency, the modulator provides a periodic loss. A pulse will form in such a way to minimize the modulator loss. Unlike the ideal shutter, which has infinite loss for all time except the desired pulse duration, the

modulator's periodic loss profile is slowly-varying. Thus, active modelocking

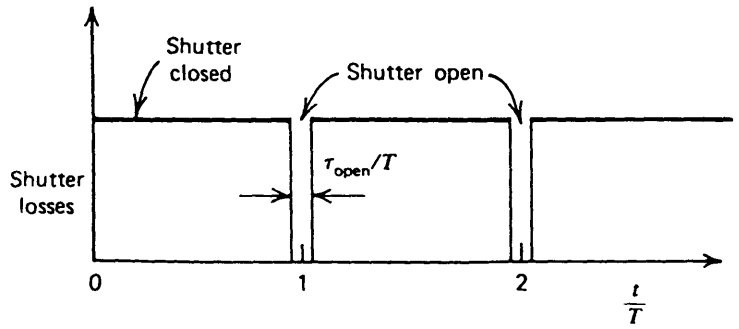

Figure 1-1: Modelocking via an ideal shutter

with sinusoidal modulation can only provide weak modelocking effects, and cannot generate sub-picosecond pulses[2].

Passive modelocking, which utilizes a saturable absorber, has been very successfully used to obtain sub-picosecond pulses. The loss of a saturable absorber decreases with increasing intensity. Since its low-intensity "wings" are attenuated more than its high intensity center, a pulse passing through a saturable absorber is narrowed. Significant changes in the loss profile of a saturable absorber can occur on the time scale of the pulse width, thus generating strong modelocking effects. A physical example of a saturable absorber is an organic dye[3]. Artificial saturable absorbers can be engineered using techniques such as additive pulse modelocking (APM) [4]-[5]. In this thesis, the investigated modelocked lasers will be APM lasers with erbium-doped fiber as the gain medium.

1.2 Noise of modelocked lasers

Noise is present in the output of the modelocked laser. Some of the noise sources are gain fluctuations, length and refractive index fluctuations, and the amplified spontaneous emission (ASE) fluctuations. These sources induce small changes, from pulse to pulse, in timing (timing jitter), energy, phase, carrier frequency, width, and in some systems, chirp. A thorough understanding of the noise mechanisms is needed to minimize the fluctuation.

Theoretical studies have been done on the noise of modelocked lasers. D. von der Linde's work has shown that the noise can be characterized by measuring the power spectrum of the photodetector current[6]. The noise characteristics of many lasers systems, such as the color-center lasers, the colliding-pulse lasers, and Ti:sapphire lasers, have been characterized using this phenomenological approach[7]-[10]. However, D von der Linde's study has not considered the physical origins which give rise to these types of noise. Furthermore, his paper has not emphasized the interplay between different types of noise, e.g. pulse amplitude fluctuation and carrier frequency noise.

Assuming weak saturable absorber action, Haus and Mecozzi proposed a perturbational approach to treat the noise of passively modelocked soliton lasers, an approach which is closely related to the soliton perturbation theory. Equations of motion for different types of noise have been derived. Expressions for timing, amplitude, phase and frequency noise at the quantum limit have been obtained[11]. In this thesis we review the Haus-Mecozzi theory and report the successful observation of this quantum-limited timing jitter in an all-fiber soliton ring laser. Haus and Namiki have also proposed a theory to account for the noise of the stretched pulse ring laser. This theory and its supporting experimental evidences is also included in this thesis.

1.3 Applications of Modelocked Lasers

Potential applications of ultrashort optical pulses span from medical fields to telecommunication industry; from solid state physics to precision instrumentation. For example, optical coherence tomography (OCT) has been used for depth imaging in the eye[12]-[13]. In this case a fiber laser has an advantage in power over LED, the most widely used source for OCT. This power gain may prove immediately useful in this context.

These modelocked lasers may also find use in optical sampling systems where the profiles of longer pulses(hundreds of femtoseconds to picosecond durations) are observed by cross-correlating them with a shortened pulse. Such systems may become important if

the research in time-division multiplexed (TDM) terrabit communications continues, as they allow direct observation of terrabit data sequences at resolutions much higher than those achievable with streak cameras[14].

A third possible application for modelocked lasers is in precision measurements. Interferometric schemes are ubiquitous in spectroscopy and in the measurement of the optical properties of partially transmitting samples. Interferometers also have numerous applications such as ultra-sensitive motion sensors. Under certain conditions such as short integration time and low light levels, interferometers can become limited by the shot noise. The way to overcome this limit is to use squeezed light. If nonlinear mechanisms are used for squeezing, using pulses is more advantageous than using cw light since the high peak power of the pulse allows it to experience more nonlinear effects[15]-[18]. The hope to use squeezed optical pulses to operate an optical fiber gyroscope has been the main motivation for the funding and the research done on squeezed states at MIT and is an ongoing project in our group[19].

To successfully utilize modelocked lasers in most of the applications mentioned above, one must make sure that these lasers are not noisy. The goal of being able to engineer quiet modelocked lasers motivated a thorough investigation of the noise mechanisms in these lasers. The results of this investigation are presented in this thesis.

1.4 Organization of Thesis

The rest of this thesis will be organized as follows. Chapter 2 reviews the theory of additive pulse modelocking. The chapter will concentrate on the soliton laser and the stretched pulse laser. Chapter 3 discusses the noise theory. The basics of stochastic processes are reviewed. D. von der Linde's phenomenological approach to the noise of modelocked lasers is presented. The Haus-Mecozzi noise theory for the soliton laser and the noise theory for the stretched pulse ring laser are then discussed. Chapter 4 presents the experimental results for both the soliton laser and the stretched pulse laser, and compares them with

each other and with the theories. Chapter 5 ends this thesis with summary and future work.

Chapter 2

The Theory of Additive Pulse Modelocking (APM) in Fiber Lasers

The theory of APM is briefly reviewed in this chapter. Special attention is devoted to the analytic theories of the soliton laser and the stretched pulse laser.

2.1 Additive Pulse Modelocking (APM)

A saturable absorber, whose loss decreases with increasing optical intensity, is used in passive modelocking. A pulse passing through a saturable absorber modulates its own amplitude (Self Amplitude Modulation) and in turn, shortens itself. Because of the fast response time of these saturable absorbers, passive modelocking can generate femtosecond pulses. However, it is often difficult to find suitable absorbing material, the performance of which limits the performance of the modelocking system.

The discovery of artificial saturable absorber (ASA) by Mollenauer and Stolen [20] in 1984 and the subsequent theoretical studies by Haus [4], [5], [21], [22] revolutionized passive modelocking. Mollenaur's soliton laser is shown in Figure 2-1a. It contains two coupled resonant cavities: one is the laser cavity for a synchronously pumped color-center laser, and the other contains an optical fiber whose purpose is to shape the pulses

into solitons. The sync-pumped system typically gives 8ps pulses, but the external cavity shortened these pulses to sub-picosecond ones.

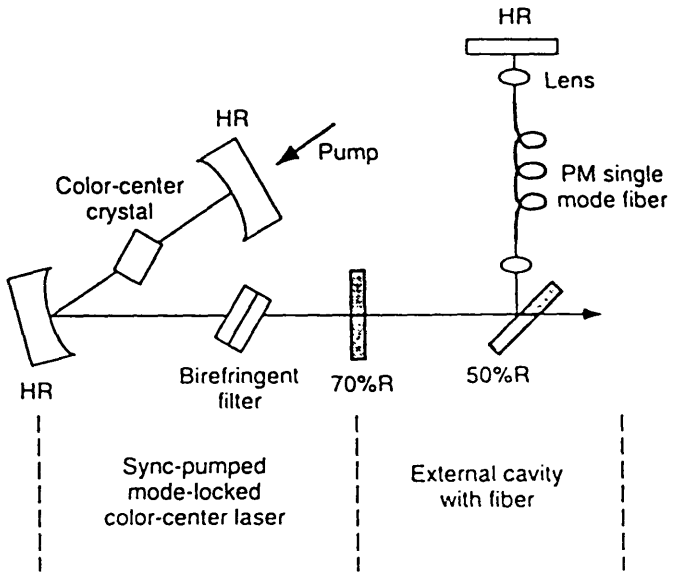

Figure 2-1a, The Soliton Laser by Mollenauer et al.

This nonlinear interference between the laser cavity and an auxiliary cavity is the underlying principle of ASA, now termed Additive Pulse Modelocking (APM). Figure 2-1b contains a generalized schematic of APM[5]. The auxiliary cavity is on side two of the mirror. The equations for the wave amplitudes at the mirror are

$$b_1 = ra_1 + \sqrt{1-r^2}a_2 \tag{2.1}$$

$$b_2 = \sqrt{1-r^2}a_1 - ra_2 \tag{2.2}$$

where the a_i's are the incident waves and the b_i's are the reflected waves at the mirror. Wave $b_2(t)$, the time envelope of the reflected wave on side 2, travels through the nonlin-

ear medium, is attenuated by the factor L, and returns as wave a_2. Ignoring dispersion in the auxiliary cavity, and suppressing the round-trip delay, a_2 is related to b_2 by

$$a_2(t) = L\exp -j\{\phi + \kappa[a_2(t)^2 - a_2(0)^2]\} b_2(t) = L\exp[-j(\phi+\Phi)]\, b_2(t) \quad (2.3)$$

where t=0 is the peak of the pulse and Φ is the phase shift induced by the nonlinearity

$$\Phi \equiv \kappa[a_2(t)^2 - a_2(0)^2], \quad (2.4)$$

κ is a parameter that is proportional to the length of the fiber and the nonlinear index, and ϕ is the phase shift of the carrier on reflection. Combining (2.1), (2.2) and (2.3), one obtains

$$b_1 = \frac{1}{\sqrt{1-r^2}}\{1 + \frac{r}{L}\exp[j(\phi+\Phi)]\}\, a_2 \quad (2.5)$$

$$a_1 = \frac{1}{\sqrt{1-r^2}}\{r + \frac{1}{L}\exp[j(\phi+\Phi)]\}\, a_2 \quad (2.6)$$

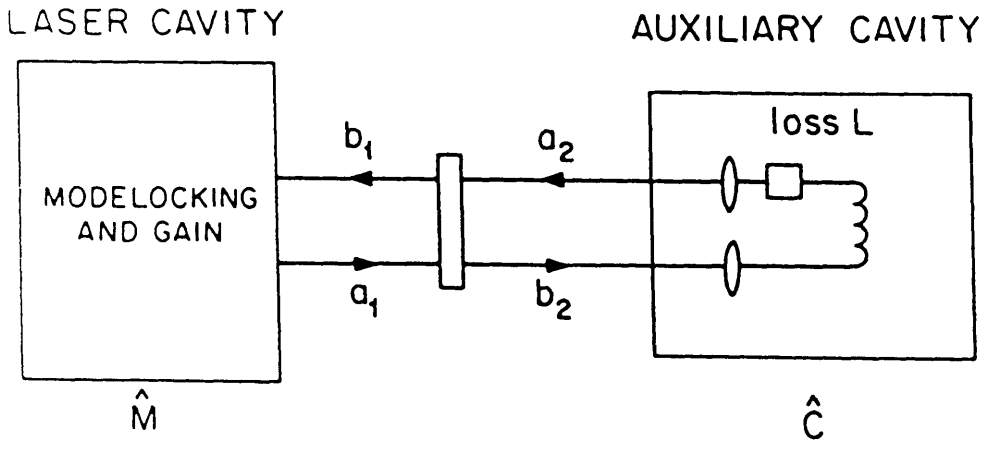

Figure 2-1b Schematic of laser cavity and auxiliary cavity

The reflection coefficient from Equations (2.5) and (2.6) is:

$$\Gamma = \frac{b_1}{a_1} = \frac{1 + \frac{r}{L}\exp\left[j\left(\phi + \Phi\right)\right]}{r + \frac{1}{L}\exp\left[j\left(\phi + \Phi\right)\right]} \tag{2.7}$$

Assuming small L and small Φ, one obtains

$$\Gamma = r + L\left(1 - r^2\right)e^{-j\phi}\left(1 - j\Phi\right) \tag{2.8}$$

When ϕ=-π/2 and Φ goes negative, then the reflection decreases. Φ, as defined in (2.4), equals to zero at the peak and goes negative in the wings. Thus reflection is maximum at the pulse center and decreases in the wings. An ASA is constructed and the pulse shortens.

2.1.1 Polarization APM

The lasers studied in this thesis utilizes polarization APM [23], [24]. The basic idea of polarization APM is illustrated in Fig. 2-2. Elliptically polarized light rotates in the Kerr medium, a fiber in this thesis, at an angular rate per unit distance proportional to the optical intensity. A properly aligned polarizer transmits higher intensity with less loss. This effect can be used to make an ASA. Too much rotation will begin to increase the loss again, and a transmission characteristic similar to that of the Michelson interferometer will develop as a function of net phase. The passive modelocking of fiber lasers using this effect was first experimentally demonstrated by Hofer et al.[23] and is now well-established.

ASA based on nonlinear polarization may still be thought of as APM. Elliptical polarization may be broken down into the circular polarization eigenstates: left and right hand circular. So in the case of polarization APM in the ring laser the two signals that form the arms of the interferometer are the two circular eigenstates. The differential nonlinear phase shift between them results in the ellipse's rotation [24].

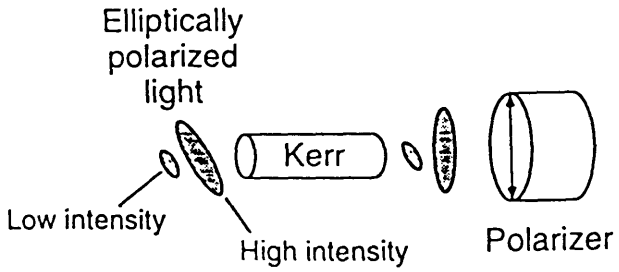

Figure 2-2: Nonlinear polarization rotation for artificial saturable absorption

2.2 Analytic Theory of Fiber Soliton Ring Lasers

2.2.1 Laser Schematic

A schematic of the all-fiber soliton ring laser is shown in Fig. 2-3. The laser has a simple but very robust design: it consists only of erbium-doped fiber(EDF), standard single mode fiber(SMF-28), and two "rabbit-ear" polarization controllers. A Faraday isolator is inserted to force unidirectional operation [26]-[28]. The polarization controllers and the polarizer produce APM action by transforming linear polarization into elliptic polarization, followed by SPM in the fiber, which rotates the ellipse. The polarizer transforms the rotation of the ellipse into amplitude modulation. The system in Fig. 2-3 uses a second polarization controller to compensate for the spurious polarization in the non-polarization maintaining fiber. Moreover, since the excited states of the erbium ions have very long relaxation times, the ring laser is not sensitive to the pump noise and gain fluctuation except at very low frequencies. These features make the ring laser particularly attractive for noise studies.

2.2.2 Nonlinear Schroedinger Equation(NLSE) [29]

The most important factors affecting the pulse propagation in fiber are group velocity dis-

persion(GVD) and self phase modulation(SPM). Waves of different frequencies travel at

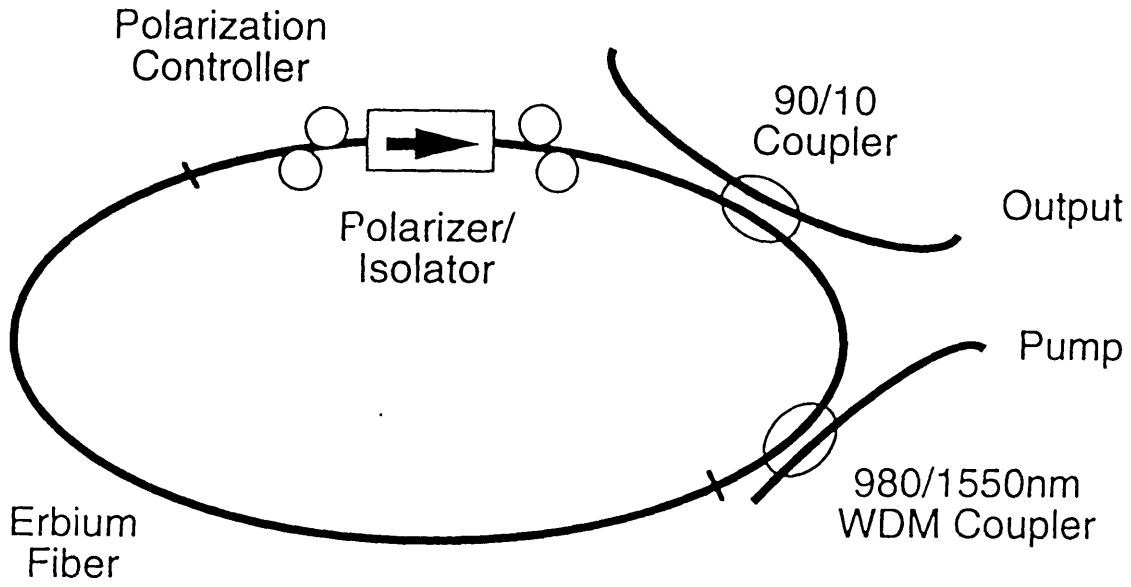

Figure 2-3: All fiber soliton laser schematic

different speeds because of GVD. Expanding the propagation constant $\beta(\omega)$

$$\beta(\omega) = \beta_o + \beta'\omega + \frac{1}{2}\beta''\omega^2 + \ldots \tag{2.9}$$

β" is the GVD. When β" is positive, the GVD is said to be normal. In the normal regime the lower frequency radiation travels faster. The GVD is anomalous when it is negative and higher frequency radiation travels faster. SMF-28, for example, has anomalous GVD. In the circular basis suitable for polarization APM, SPM in an isotropic Kerr medium can be quantifies as

$$\kappa = \frac{4\pi n_2 d}{\lambda A_{eff}} = 2\eta d \tag{2.10}$$

where n_2 is the nonlinear index, d is the length of the Kerr medium, λ is the wavelength,

and A_{eff} is the effective area. Pulse propagation in fiber is governed by the nonlinear Schrodinger equation(NLSE).

$$j\frac{\partial a}{\partial z} = \left(-\frac{1}{2}\beta''\frac{\partial^2}{\partial t^2} + \eta|a|^2\right)a \tag{2.11}$$

where a is the field, β" is the GVD, and η is the nonlinearity. When β" <0, the solutions to the NLSE are solitons. The fundamental or N=1 soliton is given by:

$$a(z,t) = \sqrt{P_s}\,\mathrm{sech}\left(\frac{t}{\tau}\right)e^{jk_s z} \tag{2.12}$$

$$\text{where } P_s = \frac{|\beta''|}{\eta\tau^2} \tag{2.13}$$

$$k_s = \frac{\pi}{4Z_0} = \frac{\beta''}{2\tau^2} \tag{2.14}$$

A characteristic of the soliton is the area theorem:

$$Area = \pi\tau\sqrt{P_s} = \pi\sqrt{\frac{|\beta''|}{\eta}} = \int_{-\infty}^{+\infty} a(z,t)\,dt, \tag{2.15}$$

which for a set of given parameters is a constant. This constraints the pulse width and the pulse peak power. A perturbed soliton no longer satisfies the soliton area theorem and sheds dispersive radiation to readjust itself. These dispersive waves may be phase-matched and generate sharp spectral sidebands. These sidebands introduce instability and limit the nonlinear phase shift, and place an upper limit on pulse energy and width.

2.2.3 Master Equation[4]

In a modelocked laser factors other than GVD and SPM are present. For a soliton laser APM can be cast into the following master equation:

$$L\frac{\partial a}{\partial z} = \left[-l + g + \left(\frac{g}{\Omega_g^2} + jD\right)\frac{\partial^2}{\partial t^2} + (\gamma - j\delta)|a|^2 - \mu|a|^4\right]a \tag{2.16}$$

where a is the pulse envelope, L is the length of the fiber, l is the loss within the distance L,

g the gain, Ω_g the filter bandwidth, D the dispersion parameter, γ the Self-Amplitude Modulation(SAM) parameter, δ the self-Phase modulation(SPM) parameter and μ is the saturation parameter of SAM. This equation is very similar to the NLSE. If the extra terms are small, they can be treated as perturbations to the NLSE. Since the dispersion of SMF-28 is anomalous, the solution of the master equation is a perturbed soliton.

The exact solution is

$$a = A_o\left[\operatorname{sech}\left(\frac{t}{\tau}\right)\right]^{1+j\beta} \tag{2.17}$$

The chirp parameter β and the pulse width τ are constrained by

$$\beta = -\frac{3}{2}\chi + \sqrt{\left(\frac{3}{2}\chi\right)^2 + 2} \tag{2.18}$$

$$\tau_n = \frac{2 - 3D_n\beta + \beta^2}{\gamma} = \frac{-2D_n - 3\beta + D_n\beta^2}{\delta} \tag{2.19}$$

where

$$\frac{1}{\chi} = \frac{\delta + \gamma D_n}{\delta D_n - \gamma} \tag{2.20}$$

$$\tau_n = \frac{E_p \Omega_g^{\ 2}}{2g}\tau \tag{2.21}$$

$$D_n = \frac{\Omega_g^{\ 2}}{g}D \tag{2.22}$$

2.3 Analytic Theory of the Stretched Pulse Ring Laser

As mentioned before, in the case of the soliton laser the nonlinear phase shift in one round trip is determined by the pulse energy and width. This puts an upper limit on the energy achievable with a soliton of given width, since the nonlinear phase shift in one round trip

is limited by the sideband generation of a periodically perturbed soliton. Such consideration leads to the conclusion that soliton propagation in an all-fiber laser is not desirable. Preferable is a system in which the pulse maintains minimum pulse width only over portions of the length and accumulates less non-linear phase shift. This is the principle underlying stretched pulse APM, which uses segments of large positive and large negative GVD fibers in the laser cavity.

2.3.1 Laser Schematic

Figure 2-4 shows a schematic of the stretched pulse laser. The ring consists of the erbium doped amplifying fiber with positive dispersion, and a segment of passive fiber with negative dispersion. The waveplates are adjusted to provide the elliptic polarization necessary for the Polarization-Additive Pulse Modelocking (P-APM) [30].

2.3.2 Master Equation for the Stretched Pulse Laser[31], [32]

Though there are large changes in pulse width per round trip in a stretched pulse laser, an analytic theory can still be derived if the following assumption is made: the pulse can have large linear changes due to GVD in one round trip, but the nonlinear changes are required to be small. This assumption is realistic for the stretched pulse laser since the stretching of the pulse reduces the nonlinearity in the cavity.

Because of the large effects due to GVD, one starts out with a gaussian pulse circulating in the fiber ring with the gain balancing the loss and no other pulse shaping mechanisms. The pulse is transform-limited at the two mirror positions in the loop as shown in Figure 2-4. The average width of the pulse is the shortest when the positions of minimum width are centered symmetrically. The pulse experiences maximum nonlinearity, and thus maximum nonlinear pulse shaping, at these positions. Focusing on the pulse at this particular position, one can expand the APM modulation into a Taylor series in time, and keep

only up to the quadratic terms. One starts by calculating the nonlinear phase shift across

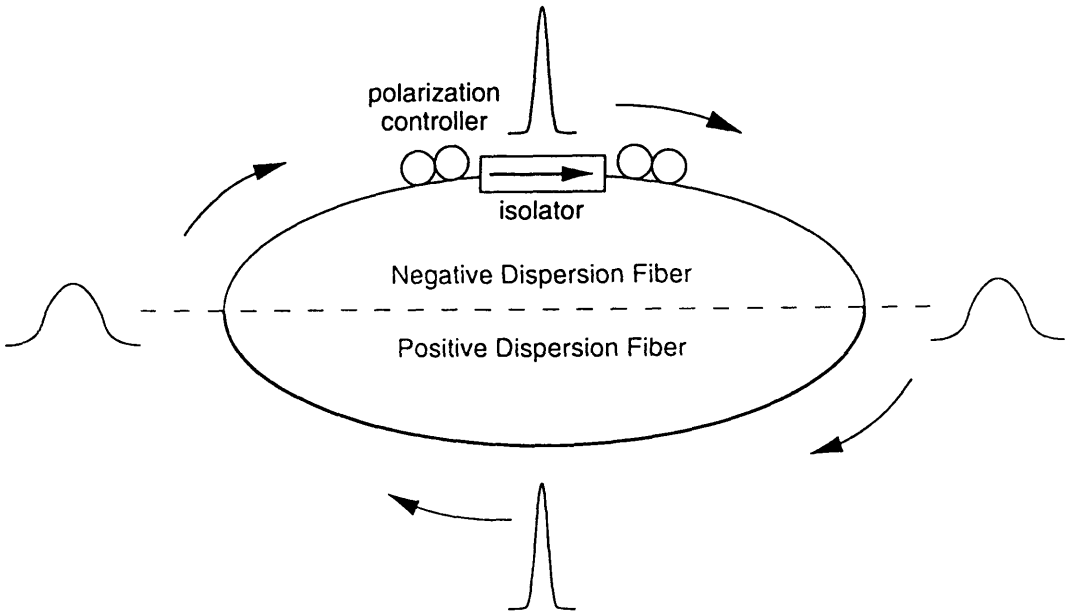

Figure 2-4: Stretched pulse laser schematic

the pulse integrated around a loop. Ignoring the nonlinear effects, one knows that the solution to the linear dispersive equation is

$$a(t,z) = \frac{A_o}{\sqrt{1+j\frac{z}{b}}}\exp\left[-\frac{t^2}{2\tau_o^{\,2}}\frac{1}{1+j\frac{z}{b}}\right] \quad \text{where} \quad b = -\frac{\tau_o^{\,2}}{\kappa''} \tag{2.23}$$

To take SPM into account, one writes A_o as a function of z:

$$A_o = |A_o|e^{-j\Phi(z)}. \tag{2.24}$$

Here Φ is the nonlinear phase shift and is expressed as:

$$\Phi = 4\kappa|A_o|^2|b|\int_0^{L/(2b)}\frac{1}{\sqrt{1+x^2}}e^{-\frac{t^2}{\tau_o^2}\frac{1}{1+x^2}}dx \tag{2.25}$$

Figure 2-5 shows that a parabolic approximation could describe the phase dependence over most of the pulse interval. So the phase can be expanded into a Taylor series and be truncated at the quadratic term. The APM action is proportional to the nonlinear phase, and can also be approximated by a parabola. Combining the effects of gain(g), loss(l), dispersion(D), gain dispersion($g/\Omega g^2$), SPM(δ) and APM, one derives the following master equation for the stretched pulse laser:

$$T_R \frac{\partial a}{\partial T} = \left[-l + g + \left(\frac{g}{\Omega_g^2} + jD \right) \frac{\partial^2}{\partial t^2} + (\alpha - j) \left[\Phi_o - |\mathrm{Ao}|^2 \delta t^2 \right] \right] a \tag{2.26}$$

where $\Phi = \Phi_o - |\mathrm{Ao}|^2 \delta t^2$, with $\Phi = |A_o|^2 \tau^2 \delta \log \left| \frac{2Lk''}{\tau_o^2} \right|$, and A_0 the pulse amplitude, is the nonlinear phase shift. α is a proportionality factor which, when multiplied by the nonlinear phase, represents the APM action; and a net group velocity dispersion exists due to an imbalance between positive and negative dispersion contributions of the two fiber segments.

The steady state solution to (2.26) is a gaussian with a chirp parameter(β),

$$a = A_o e^{-\frac{t^2}{2\tau^2}(1 + j\beta)} \equiv u_o(t) \tag{2.27}$$

with

$$(g - l) - \left(\frac{g}{\Omega_g^2 \tau^2} + j \frac{D}{\tau^2} \right) (1 + j\beta) + (a - j) \Phi_o = j\psi \tag{2.28}$$

and

$$\left(\frac{g}{\Omega_g^2 \tau^4} + j \frac{D}{\tau^4} \right) (1 + j\beta)^2 = (\alpha - j) |A_o|^2 \delta \tag{2.29}$$

From (2.27)-(2.29) two observations can be made. First of all, the product $|A_0|^2\tau^4$ is fixed. Thus the area theorem for the stretched pulse laser is that the integral of $\sqrt{a_o(t)}$ over time is constant for a given set of parameters. Secondly, the amplitude, width, and chirp of the

steady state pulse obeys the following relation:

$$\beta = \tan\left\{\frac{1}{2}\arg\left[\frac{(\alpha - j)}{\frac{g}{\Omega_g^{\,2}} - jD}\right]\right\} \tag{2.30}$$

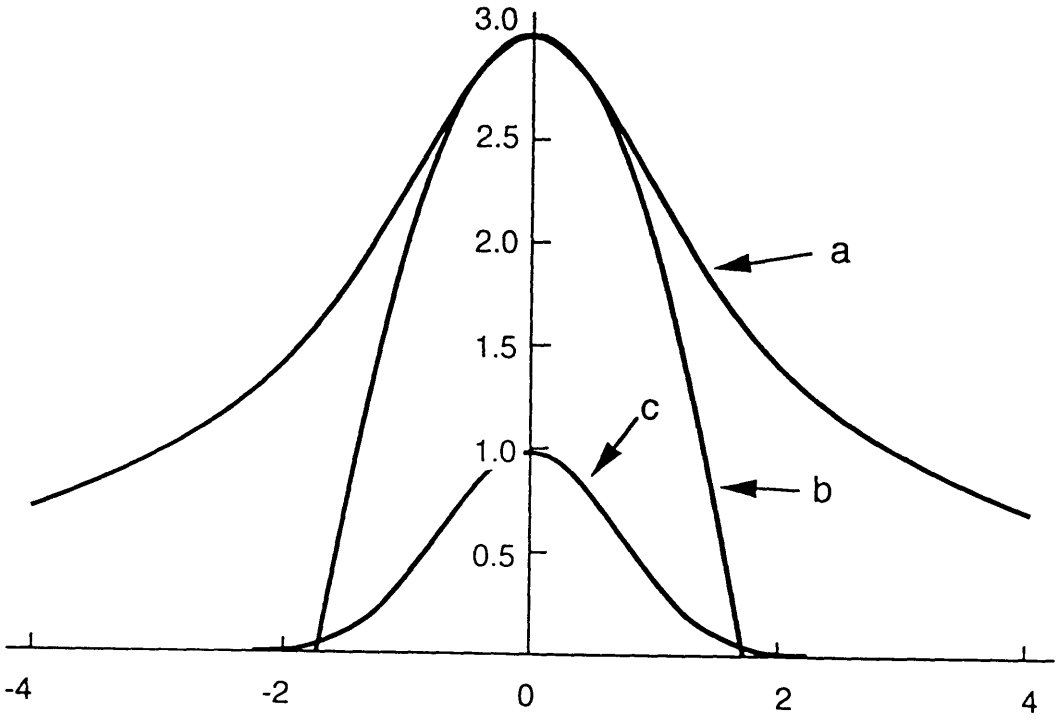

Figure 2-5: Parabolic phase dependence over the pulse profile

Chapter 3

Noise of Modelocked Lasers

This chapter will start with a brief review of stochastic processes. Then it will go to D. von der Linde's treatment of noise. This first order theory applies to all the continuously-operating modelocked lasers. However, this approach only allows a quantification of the noises and does not give any insight into the noise mechanism. The Haus-Mecozzi theory for the soliton laser and Haus' theory for the stretched pulse laser will then be reviewed and compared. Their physical implications will be discussed.

3.1 Stochastic Processes[33],[54]

There are a few ways to view a stochastic process. On one hand one may consider a stochastic process as a collection of random variables indexed in time. In the case of a discrete-time process there are countably infinite number of such random variables. For a continuous-time process a continuum of random variables must be used.

Another way to view a stochastic process is to express it as a function of x(t,w), where t is the time index, and w is the event index. Viewed this way, $x(t_0,w)$ with $t=t_0$ fixed represents a random variable at the corresponding instant in time. At $w= w_0$, however, $x(t,w_0)$ becomes a particular realization of the stochastic process, or a sample path. Therefore, one can think of this process as describing experiments, the outcomes of which

yield the entire sample paths. From here on the w dependence in our notation will be dropped and x(t) will be used.

In general, one needs joint probabilistic description of the stochastic process at different times to obtain its complete characterization. However, the processes studied in this thesis are independently and identically distributed white noise with a gaussian probability distribution. The mean and the (auto)covariance are sufficient to completely determine this type of process. The mean and the covariance are defined as

$$m_x(t) = E[x(t)] \tag{3. 1}$$

$$R_{xx}(\tau) = E[x(t)\,x(t+\tau)] \tag{3. 2}$$

where $E[x] = \int xP(x)\,dx$, and P(x) is the probability distribution of the random variable x. When measuring the process characteristics in this thesis, one also assumes that the process is ergodic, i.e. the time-averaged quantities are accurate representation of the ensemble-averaged statistics. So E[x]'s in (3. 1) and (3. 2), when measured in the laboratory, denote time averages, and will be denoted by "<>" from here on.

The power in a random process is distributed as a function of frequency. The power spectral density(psd), or the power spectrum, is used to quantify this distribution. The power spectrum is formally defined as follows:

Let h(t) be the impulse response of a unit-energy, deal bandpass filter whose frequency response is $H(j\Omega) = \sqrt{2\pi/\varepsilon}$ for $|\omega-\omega_0| < \varepsilon/2$, and zero otherwise, and let x(t) denote the output of this filter when its input is the random process x(t), then the power spectral density of the process x(t) at $\Omega=\Omega_0$ is $<|X(j\Omega)|^2> = \lim_{\varepsilon->0} \text{var } x(t)$.

The power spectrum is related to the autocorrelation function via the Wiener-Khinchine Theorem:

$$P_x(\omega) \equiv <|X(j\Omega)|^2> = \int_{-\infty}^{+\infty} R_{xx}(\tau)\,e^{-j\Omega\tau}d\tau \tag{3. 3}$$

i.e., the autocorrelation function and the power spectrum are Fourier transform pairs.

Because of the availability of highly sensitive and accurate RF spectrum analyzers, noise will be studied exclusively via the power spectrum in this thesis.

3.2 A Phenomenological Approach to the Noise of Mode-locked Lasers[6]

D. von der Linde treats laser noise as uncorrelated first order deviations from an ideal pulse train. Let the output of the laser intensity of an imperfectly modelocked laser be:

$$F(t) = \Sigma_{\mu} f\left(t + \mu T_R\right) + \delta F(t) \tag{3.4}$$

where f(t) is the temporal intensity profile of the individual pulses in the train, T_R is the pulse round trip time, and $\delta F(t)$ represents the fluctuation. In the case of Fourier transform-limited pulses, the noisy laser output to first order can be written as:

$$F(t) = F_o(t) + F_o(t)A(t) + F_o'(t)T_R J(t) \tag{3.5}$$

The first term in (3. 5) is the output of a perfectly modelocked laser; the second term represents amplitude noise of the laser pulses; and the last term represents the timing jitter with J(t) being the relative deviation from the average pulse round-trip time T. Random nature of the laser noise leads to the following power spectrum:

$$P_F(\omega) = P_{Fo}(\omega) \otimes \left[\delta(\omega) + P_A(\omega)\right] + \left[\left(\omega T_R\right)^2 P_{Fo}(\omega)\right] \otimes P_J(\omega) \tag{3.6}$$

where $P_A(w)$ and $P_J(w)$ are the power spectra of A(t) and J(t), respectively. Substituting

$$P_{FO}(\omega) = \left(\frac{2\pi}{T_R}\right)^2 |f(\omega)|^2 \Sigma\delta\left(\omega - \frac{2\pi\nu}{T_R}\right) \tag{3.7}$$

into (3.6), one obtains the final expression for the power spectrum of the noisy laser:

$$P_F(\omega) = (2\pi/T_R)^2|f(\omega)|^2\Sigma_\mu\left[\delta(\omega_\mu) + P_A(\omega_\mu) + (2\pi\mu)^2 P_J(\omega_\mu)\right] \quad (3.8)$$

where $\omega_\mu=(\omega-2\mu/T_R)$, and μ is an integer running from minus to plus infinity.

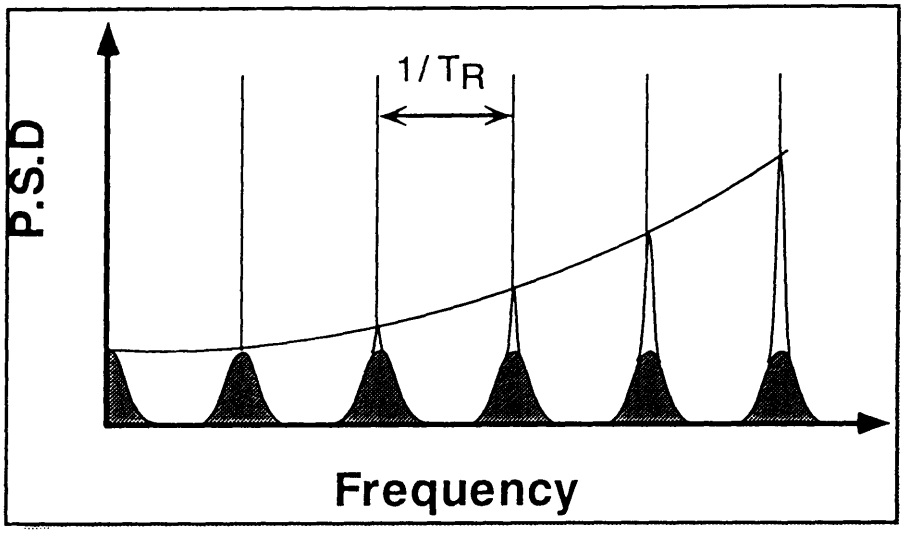

Figure 3-1: Noise structures of modelocked lasers,
shaded=energy fluctuation, clear=timing jitter

Equation (3. 8) is illustrated in Fig. 3-1: the summation over μ represents a series of frequency structures(harmonics) centered around ω_μ with constant spacing $\Delta\omega=2\pi/T$. Each structure has three parts. The output from an ideal modelocked laser is the delta function term. The amplitude fluctuation is represented by the second term. The third term is the power spectrum of the timing jitter. Notice that the jitter structure is proportional to μ^2, where μ is the individual frequency harmonic. This dependence allows one to extract the power spectra for both the timing jitter and the amplitude noise. When $\mu=0$, the jitter

term vanishes, and the amplitude noise can be measured. On the other hand, the noise spectrum around the higher order harmonics is dominated by $P_J(\omega)$, and the jitter can then be extracted.

In this thesis, the noise is assumed to be zero mean, and the autocovariance with τ =0, or the root mean square(r.m.s.) deviation, is used to quantify the noise. By Parseval's Theorem:

$$(\Delta E/E)^2 = \langle A^2 \rangle = \int_{-\infty}^{+\infty} P_A(\omega)\, d\omega \tag{3.9}$$

$$(\Delta t/T)^2 = \langle J^2 \rangle = \int_{-\infty}^{+\infty} P_J(\omega)\, d\omega \tag{3.10}$$

where E is the average pulse energy, and T is the laser cavity round-trip time.

3.3 The Haus-Mecozzi Noise Theory for the Soliton Laser[11]

The Haus-Mecozzi theory starts with the master equation for modelocking:

$$T_R \frac{\partial a}{\partial T} = \left[-l + g\left(1 - \frac{1}{\Omega_g}\frac{\partial}{\partial t} + \frac{1}{\Omega^2_g}\frac{\partial^2}{\partial t^2} \right) + jD\frac{\partial^2}{\partial t^2} + (\gamma - j\delta)|a|^2 \right] a + T_R S(t, T) \tag{3.11}$$

Here, T_R is the round trip time; a(T,t) is the electric field amplitude in the resonators, T is a time variable on the scale of many cavity round-trip times; l is the incremental loss, g is the incremental gain per pass, Ω_g is the gain bandwidth; γ is the effective saturable absorber action that is produced by APM, δ is the Kerr phase modulation, D is the group

velocity dispersion(GVD); and S(t,T) is the noise source[1]. Aside from the noise source, (3.11) is essentially the same as (2.15). Trying the ansatz

$$a(t,T) = [a_s(t-t_o) + \Delta a(t-t_o,T)]\exp\left(-j\frac{\delta}{2}A_o{}^2\frac{T}{T_R}\right) \tag{3.12}$$

where $a_s(t) = A_o\,\mathrm{sech}\left(\frac{t}{\tau}\right)$, τ is the pulse width, Haus and Mecozzi have obtained an equation of motion for Δa, the laser fluctuation.

$$T_R\frac{\partial}{\partial T}\Delta a(t-t_o,T) = \left\{\left(g - l + j\frac{\delta}{2}A_o{}^2 + \left(\frac{g}{\Omega_g{}^2} + j|D|\right)\frac{\partial^2}{\partial t^2}\right) + \right. \tag{3.13}$$

$$\left. 2(\gamma - j\delta)a_s{}^2(t-t_o)\right\}\Delta a + (\gamma - j\delta)a_s{}^2\Delta a^* - g_s\left(1 - \frac{1}{\Omega_g}\frac{\partial}{\partial t} + \frac{1}{\Omega^2{}_g}\frac{\partial^2}{\partial t^2}\right)$$

$$\frac{a_s(t)}{2\tau A_o{}^2}\int dt a_s(t)\,(\Delta a + \Delta a^*) + T_R S(t,T)$$

where

$$g_s = \frac{g_o}{P_s T_R}\frac{2\tau A_o{}^2}{\left\{1 + \frac{2\tau A_o{}^2}{P_s T_R}\right\}^2}.$$

the above equation differs slightly from the one in the original paper in that we no longer assume the condition $\frac{\gamma}{\delta} = \frac{g/\Omega_g{}^2}{-D}$ to hold. This generalization is possible when both the filtering and the APM action may be considered small perturbations of the soliton shaping. This assumption is particularly well-satisfied in fiber lasers.

For convenience pulse energy is introduced and defined as

$$w_o = \int a_s{}^2(t)\,dt = 2A_o{}^2\tau. \tag{3.14}$$

Expanding the noise in terms of fluctuations of pulse energy(Δw), phase($\Delta\theta$), timing(Δt), and frequency(Δp, -$p=\omega-\omega_0$, the deviation from the angular carrier frequency) and using the corresponding adjoint functions, one may project out the individual noise component associated with each fluctuation from Δa, and derive its equations of motion. These equations are listed below:

$$T_R\frac{\partial}{\partial T}\Delta w = \left[-2g_s + \frac{8}{3}\gamma A_o^{\,2} - \frac{2}{3}\frac{g}{\Omega_g^{\,2}}\frac{\delta}{|D|}A_o^{\,2}\right]\Delta w + T_R S_w(T) \tag{3.15}$$

$$T_R\frac{\partial}{\partial T}\Delta\theta = -\delta A_o^{\,2}\frac{2\Delta w}{w_o} + T_R S_\theta(T) \tag{3.16}$$

$$T_R\frac{\partial}{\partial T}\Delta p = \left(-\frac{4}{3}\frac{g}{\Omega_g^{\,2}\tau^2}\right)\Delta p + T_R S_p(T) \tag{3.17}$$

$$T_R\frac{\partial}{\partial T}\Delta t = -2|D|\Delta p - \frac{g}{\Omega_g}\frac{\Delta w}{w_o} + T_R S_t(T) \tag{3.18}$$

The noise sources $S_i(T)$ are defined by projecting the respective adjoint functions onto the noise source S(t,T).

Equation (3.15) shows how the pulse can reach its steady state energy: APM provides an intensity dependent gain which favors the transmission of high-intensity portion of the pulse. The pulse energy grows exponentially until gain saturation and filtering loss, both of which increase with pulse energy, become large enough to suppress this nonlinear gain. There may be other mechanisms such as saturation of APM mechanism and continuum generation which may provide more effective pulse energy stabilization. For the sake of simplicity, the Haus-Mecozzi model neglects these mechanisms but it can be easily extended to include them as well.

According to (3.16), an energy change affects the Kerr phase shift, thus couples to the phase evolution. (3.17) shows that frequency deviations damp out because the gain of a pulse whose center frequency is off the gain line center is nonuniform across the spectrum and pushes the spectrum back to line center. (3.18) shows the relationship between the timing jitter and other fluctuations. Because of GVD, a change in pulse frequency deviation changes the group velocity. A change in pulse energy also changes the group velocity, through the Kramers-Kronig relation, i.e., change in the gain profile of the EDF also changes its index profile.

To solve (3.15)-(3.18), we first define the Fourier transform pair as

$$f(\Omega) = \frac{1}{\sqrt{T_o}}\int dT e^{-j\Omega T} f(T)\ ; \quad f(T) = \frac{\sqrt{T_o}}{2\pi}\int d\Omega e^{j\Omega T} f(\Omega) \tag{3.19}$$

where the long normalization time T_0 has been introduced to avoid the divergence of the spectrum. We then define the two relaxation times:

$$\frac{1}{\tau_w} = -\left[-2g_s + \frac{8}{3}\gamma A_o^{\,2} - \frac{2}{3}\frac{g}{\Omega_g^{\,2}|D|}A_o^{\,2}\right]\frac{1}{T_R}; \tag{3.20}$$

$$\frac{1}{\tau_p} = \frac{4}{3}\frac{g}{\Omega_g^{\,2}\tau^2}\frac{1}{T_R} \tag{3.21}$$

The energy fluctuations spectrum is

$$<|\Delta w(\Omega)|^2> = \frac{<|S_w(\Omega)|^2>}{\left(\Omega^2 + 1/\tau_w^{\,2}\right)} \tag{3.22}$$

the frequency fluctuations spectrum is

$$<|\Delta p(\Omega)|^2> = \frac{<|S_p(\Omega)|^2>}{\left(\Omega^2 + 1/\tau_p^{\,2}\right)} \tag{3.23}$$

the timing jitter spectrum is:

$$<|\Delta t(\Omega)|^2> = \frac{4D^2}{T_R^{\,2}\Omega^2}\frac{<|S_p(\Omega)|^2>}{\left(\Omega^2 + 1/\tau_p^{\,2}\right)} + \frac{g^2}{\Omega^2\Omega_g^{\,2}T_R^{\,2}}\frac{<|\Delta w(\Omega)|^2>}{w_o^{\,2}} + \frac{<|S_t(\Omega)|^2>}{\Omega^2} \tag{3.24}$$

The asymptotic behavior for large T is determined by the leading singularity, which has a spectrum of the form $1/\Omega^2$. This corresponds to the random walk, of which the r.m.s. value is of the form: $<|\Delta t(T+T_o) - \Delta t(T_o)|^2> = D_t T$, where D_t is a diffusion constant.

The phase noise spectrum is

$$<|\Delta\theta(\Omega)|^2> = \frac{\left(\delta A_o^{\,2}\right)^2}{T_R^{\,2}\Omega^2}\frac{<|S_w(\Omega)|^2>}{\left(\Omega^2 + 1/\tau_w^{\,2}\right)} + \frac{<|S_\theta(\Omega)|^2>}{\Omega^2} \tag{3.25}$$

When the pulse train impinges on a photodetector, the kth Fourier component of the detector current is produced by the beat of two Fourier components of the field amplitude that are k components apart. Summing over all possible combinations of such beat and expanding to first order, we obtain the following expression for the kth component of the detector current:

$$i_k(T) = A\left[1 + \frac{\Delta w}{w_o}\right]e^{-jk\Omega_o\Delta t} \tag{3.26}$$

where A is a scaling constant, and $\Omega_o = 2\pi/T_R$.

If the timing jitter is small, then one can expand the exponential in (2. 16),

$$i_k(T) = A\left[1 + \frac{\Delta w(T)}{w_o}\right][1 - jk\Omega_o\Delta t(T)] \tag{3.27}$$

The corresponding power spectrum is

$$<|i_k(\Omega)|^2> = A^2\left\{2\pi\delta(\Omega) + \frac{1}{w_o^2}<|\Delta w(\Omega)|^2> + k^2\Omega_o^2<|\Delta t(\Omega)|^2> + \right. \quad . \qquad (3.28)$$

$$\left. jk\Omega_o[<\Delta t^*(\Omega)\Delta w(\Omega)> - <\Delta t(\Omega)\Delta w^*(\Omega)>]\right\}$$

The above is the same expression as that derived by D. von der Linde[6] neglecting the cross-correlation terms. The amplitude noise has the same structure around each harmonic, and the timing jitter grows quadratically with k, where k labels the individual harmonics.

3.3.1 A Note on the Effects of the Finite Measurement Time on the Power Spectrum

In reality, an RF spectrum analyzer has a finite integration time so that the timing jitter power spectrum does not have a singularity at Ω=0. This can be accounted for by solving the corresponding transient problem in the time domain. Assuming that the jitter is mainly due to the frequency shift, we obtain the following from (3.17), and (3.18):

$$\Delta p(t) = e^{-t/\tau_p}\int_0^t S_p(t')\,e^{t'/\tau_p}dt' \qquad (3.29)$$

$$\Delta t(t) = -\frac{2|D|}{T_R}\int_0^t e^{-t'/\tau_p}dt'\int_0^{t'} S_p(t'')\,e^{t''/\tau_p}dt'' \qquad (3.30)$$

So the power spectrum of Δt(R) is: (3.31)

$$\frac{4D^2}{T_R^2}k^2\Omega_o^2\int_0^T e^{j\Omega t}dt\int_0^T e^{j\Omega t'}dt'\int_0^t e^{-t''/\tau_p}dt''\int_0^{t'} e^{-t'''/\tau_p}dt'''\int_0^{t''} e^{t^{IV}/\tau_p}S_p\left(t^{IV}\right)dt^{IV}\int_0^{t'''} e^{t^{V}/\tau_p}S_p\left(t^{V}\right)dt^{V}$$

Assuming that T >> τp, then the above integral gives:

for $\Omega <> 0$,

$$R = \frac{4D^2}{T_R^2}k^2\Omega_o^2 D_{pp}\left\{-\frac{\tau_p^4 T}{2+2\tau_p\Omega}+\frac{\tau_p^2 T}{\Omega^2}+\frac{(\cos(\Omega T)\tau_p\Omega-\sin(\Omega T))\tau_p^2}{\left(1+\tau_p^2\Omega^2\right)\Omega^3}-\frac{\tau_p^3}{\Omega^2}+\frac{\tau_p^5\left(\tau_p^2\Omega^2+5\right)}{4\left(\tau_p^2\Omega^2-1\right)+4\left(\tau_p^2\Omega^2\right)}\right\}$$

(3. 32)

and for Ω=0,

$$R = \frac{4D^2}{T_R^2}k^2\Omega_o^2 D_{pp}\left(\frac{\tau_p^2 T^3}{6}-\frac{\tau_p^3 T^2}{2}+\frac{\tau_p^4 T}{2}+\frac{\tau_p^5}{4}\right), \tag{3. 33}$$

where $<S_p(T)S_p(T')> = D_{pp}\delta(T-T')$.

It is found that for an RF resolution of 10 Hz(T=0.1 s) and a wide range of τp's such that T>>τp, the timing jitter structure does not deviate noticeably except near Ω=0(Figure 2).

The r.m.s. deviation of Δw and Δt are given by:

$$(\Delta w)_{rms}^2 = \frac{1}{2\pi}\int_{-\infty}^{+\infty}<|\Delta w(\Omega)|^2>d\Omega \tag{3. 34}$$

$$(\Delta t)_{rms}^2 = \frac{1}{2\pi}\int_{-\infty}^{+\infty}<|\Delta t(\Omega)|^2>d\Omega \tag{3. 35}$$

(3.34) and (3.35) are used to quantify the noise in this paper.

3.4 The Noise Theory for the Stretched Pulse Ring Laser[32]

The noise theory for the stretched pulse laser is not yet finalized. In this thesis I will

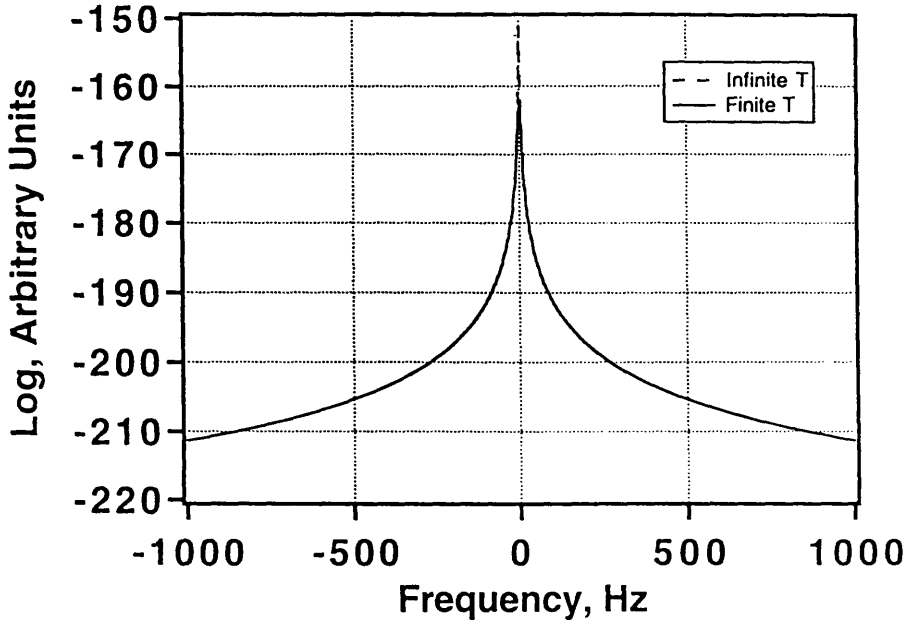

Figure 3-2: Effect of finite integration time on timing jitter, T=0.1s, τp=0.17 μs

present the derivations of the equations of motion for the perturbed pulse parameters. The implications of these equations of motion will be explored.

The perturbational approach used to develop the noise theory for the stretched pulse laser is very similar to that used for the soliton laser. One starts out by adding a noise source S(T,t) to the master equation so that (2. 22) now becomes:

$$T_R \frac{\partial a}{\partial T} = \hat{O}a + s(T,t) \tag{3. 36}$$

where $\hat{O} = \left[-1 + g + \left(\frac{g}{\Omega_b^2} + jD \right) \frac{\partial^2}{\partial t^2} + (\alpha - j)\left[\Phi_o - |Ao|^2 \delta t^2 \right] \right]$.

Perturbing (3. 36) by letting a-> a+Δa, one obtains:

$$T_R \frac{\partial}{\partial T} \Delta a = \hat{O}\Delta a + \Delta\hat{O}a + S(T,t) \tag{3. 37}$$

To solve (3. 37), one expands Δa, and project out different contributions for each

perturbation parameter using the adjoint function. One first expands Δa as a superposition of the complete set of hermite gaussians:

$$\Delta a = \sum_{n=0}^{2} c_n u_n\left(\frac{t}{\tau}\sqrt{1+j\beta}\right)e^{j\theta} + \Delta\alpha_c(T, t) \tag{3.38}$$

where u_n is the nth order hermite gaussian function, and c_n is the weight that is associated with it. The first term on the right hand side of (3. 38) represents the three lowest order hermite-gaussians and characterizes the pulse perturbation. The second term is the continuum, and will be ignored in this analysis, just like in the soliton case.

The expansion functions are defined as follows:

$$f_A(t) = u_o\left(\frac{t}{\tau}\sqrt{1+j\beta}\right) \tag{3.39}$$

$$f_\theta(t) = ju_o\left(\frac{t}{\tau}\sqrt{1+j\beta}\right) \tag{3.40}$$

$$f_t(t) = \frac{1}{2\tau}\sqrt{1+j\beta}\,u_1\left(\frac{t}{\tau}\sqrt{1+j\beta}\right) \tag{3.41}$$

$$f_p(t) = -\frac{j\tau}{2\sqrt{1+j\beta}}u_1\left(\frac{t}{\tau}\sqrt{1+j\beta}\right) \tag{3.42}$$

$$f_\tau(t) = -\frac{1}{4\tau}u_2\left(\frac{t}{\tau}\sqrt{1+j\beta}\right) \tag{3.43}$$

$$f_\beta(t) = -\frac{j}{8(1+j\beta)}u_2\left(\frac{t}{\tau}\sqrt{1+j\beta}\right) \tag{3.43}$$

Contrary to the soliton noise theory, (3. 39)-(3. 43) are not all pair wise in quadrature. Taking this into account, the adjoint projection functions are

$$\underline{f}_A^*(t) = \frac{1}{\sqrt{\pi}}\frac{\sqrt{1+j\beta}}{\tau}u_o\left(\frac{t}{\tau}\sqrt{1+j\beta}\right) \tag{3.44}$$

$$\underline{f}^{*}_{\theta}(t) = -j\frac{1}{A_o\sqrt{\pi}}\frac{\sqrt{1+j\beta}}{\tau}u_o\left(\frac{t}{\tau}\sqrt{1+j\beta}\right) \tag{3.45}$$

$$\underline{f}^{*}_{t}(t) = \frac{1}{\sqrt{\pi}}(1+j\beta)\,u_1\left(\frac{t}{\tau}\sqrt{1+j\beta}\right) \tag{3.46}$$

$$\underline{f}^{*}_{p}(t) = j\frac{1}{A_o\sqrt{\pi}}\frac{1+\beta^2}{\tau^2}u_1\left(\frac{t}{\tau}\sqrt{1+j\beta}\right) \tag{3.47}$$

$$\underline{f}^{*}_{\tau}(t) = -\frac{1}{2A_o\sqrt{\pi}}(1+j\beta)^{3/2}u_2\left(\frac{t}{\tau}\sqrt{1+j\beta}\right) \tag{3.48}$$

$$\underline{f}^{*}_{\beta}(t) = j\frac{1}{A_o\sqrt{\pi}}\frac{\sqrt{1+j\beta}}{\tau}\left(1+\beta^2\right)u_2\left(\frac{t}{\tau}\sqrt{1+j\beta}\right) \tag{3.49}$$

If the perturbation is slow, then the pulse must obey the master equation for all times. From (2.26) one deduces that β, the chirp parameter of a pulse obeying the master equation, is a constant for a set of given system parameters. Therefore β is time-invariant when the perturbation is adiabatic. Similarly, $|A_0|\tau^2$ is also invariant. This invariance implies that the change in pulse width is related to the change in amplitude via

$$\Delta A\tau^2 + 2\tau A_o\Delta\tau = 0 \tag{3.50}$$

Because of these invariances, the six perturbed pulse parameters are reduced to four. By projection, one derives the equations of motion for these four pulse parameters: pulse energy(Δw), phase($\Delta\theta$), timing(Δt), and frequency(Δp, $-p=\omega-\omega_0$, the deviation from the angular carrier frequency). They are listed below:

$$T_R\frac{\partial}{\partial T}\Delta w = 2w\left[\frac{\Delta g}{\Delta w}+\alpha\frac{\Delta\Phi_o}{\Delta w}\right]\Delta w - \frac{4}{3}\left(\frac{g}{\Omega_g^{\,2}\tau^2}+\beta\frac{D}{\tau^2}\right)\Delta w + T_R S_w \tag{3.51}$$

$$T_R \frac{\partial}{\partial T} \Delta\theta = -\Delta\Phi_o - \left[\frac{\Delta\Phi_o}{\Delta\tau} - \frac{2}{\tau}\left(\beta \frac{g}{\Omega_g^{\,2}\tau^2} + \frac{D}{\tau^2} \right) \right] \Delta\tau + T_R S_\theta(T) \tag{3.52}$$

$$T_R \frac{\partial}{\partial T} \Delta p = -4\left(1 + \beta^2 \right) \frac{g}{\Omega_g^{\,2}\tau^2} \Delta p + T_R S_p(T) \tag{3.53}$$

$$T_R \frac{\partial}{\partial T} \Delta t = 4|D|\Delta p - 4\beta \frac{g}{\Omega_g^{\,2}} \Delta p + T_R S_t(T) \tag{3.54}$$

where

$$S_i(T) = Re \int S(t, T) f_i^{\,*} \, dt \tag{3.55}$$

and

$$S_w = 2\frac{w}{A_o} S_A + \frac{w}{\tau} S_\tau \tag{3.56}$$

Notice that because the adjoint functions are not pair-wise in quadrature, certain noise sources, for example S_p and S_t, are correlated.The importance of this correlation will be discussed in Chapter 4.

The similarity between Equations (3. 51)-(3. 54) and equations (3. 15)-(3.18) are apparent. Like (3.15), (3. 51) shows that the energy fluctuation relaxes via changes in gain and the APM actions caused directly by a change in amplitude or indirectly by a change in pulse width. (3. 52) shows that the phase changes because of a change in the Kerr SPM due to a change of amplitude and pulsewidth. If the pulse if chirped, then the gain filtering affects the phase by removing the extreme frequency components. (3. 53) shows that the carrier frequency deviation is damped out by the gain filtering. Finally, (3. 54) shows that the frequency change affects the timing because of the effects due to GVD. Filtering can

shift the pulse position if the pulse is chirped and the carrier frequency deviates from the filter center frequency by removing the frequency components preferentially.

Unlike in the case of the soliton perturbation theorem, the present formalism cannot be used to treat the continuum generation of the stretched pulse laser. This is because our master equation for the stretched pulse laser contains a parabolic potential well, which is valid only over the pulse interval. The continuum lies outside of this well, and does not obey the master equation. In particular, while expanding the continuum in terms of the hermite-gaussians is valid, the dispersion relations for such expansion are not predicted by the master equation. Finding a rigorous treatment for the continuum of the stretched pulse laser is a challenge, and deserves some research efforts.

Chapter 4

Experiments on the Noise Characteristics of the APM Lasers

4.1 Experimental Setup

A 980nm diode laser is used as the pump source for the soliton laser shown in Figure 2-3. The pump power is 50 mW. The length of the ring is 4.8 meters, which leads to a 42MHz repetition rate. A Master Oscillator Power Amplifier(MOPA)[34] is used as the pump source for the stretched pulse laser shown in Figure 4-10. The pump power is 500 mW. The repetition rate is 36 MHz. Both lasers are shielded with foam to minimize length and refractive index fluctuations due to thermal effects. The remainder of the experimental setup is shown in Figure 4-1. Through a movable mirror, the collimated laser output is either sent into an HP Optical Spectrum Analyzer(OSA) to measure its optical spectrum, or a fast photodetector. The power spectrum can be obtained by feeding the photodetector output to an Advantest R3562 RF Spectrum Analyzer. No effort has been made to stabilize

the laser externally.

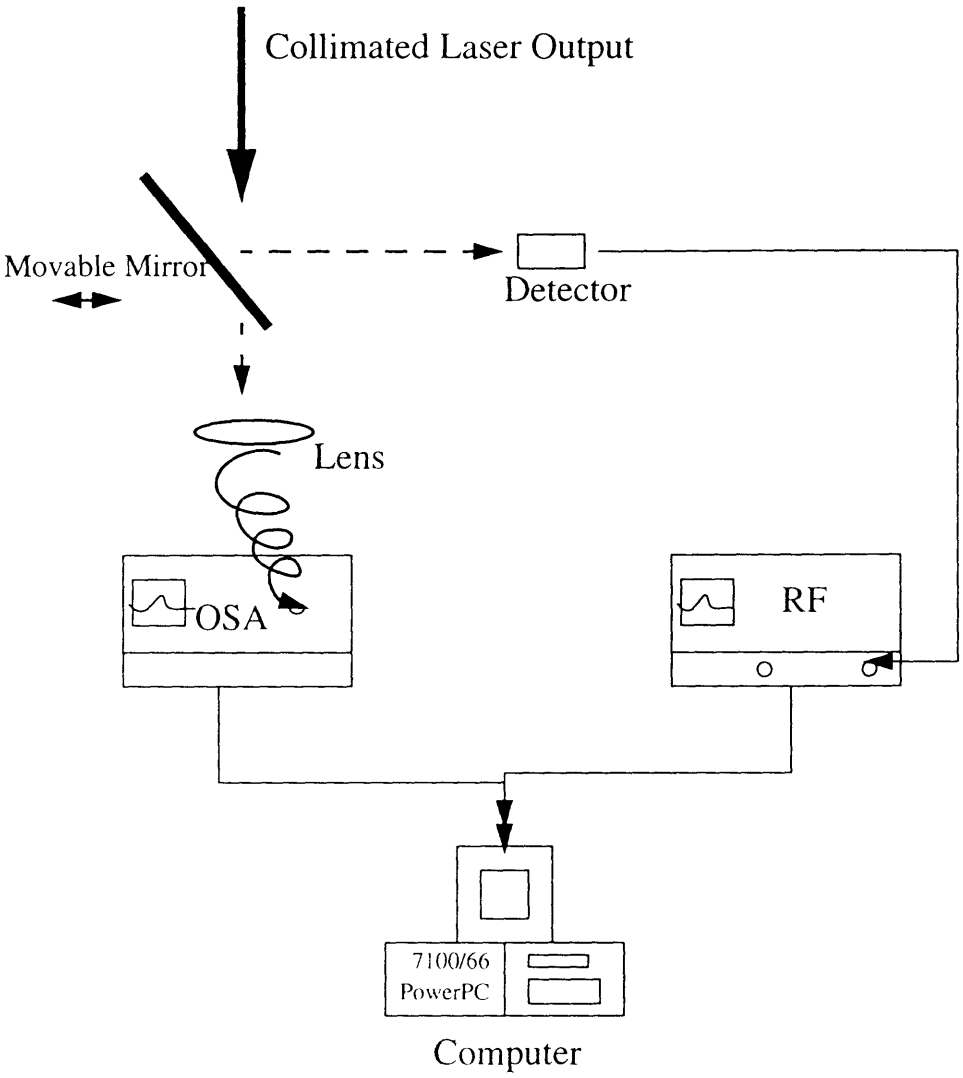

Figure 4-1: Experimental setup

4.2 Noise of the Soliton Laser

4.2.1 Experimental Results and Analysis[45], [46]

Figure 4-2, the optical spectrum of the laser output, shows that the output has Kelly sidebands but no cw light[7],[8],[35],[36]. Using these Kelly sideband and assuming a sech profile, we computed a pulsewidth (τ) of 170 fs. Autocorrelation measurement confirms this

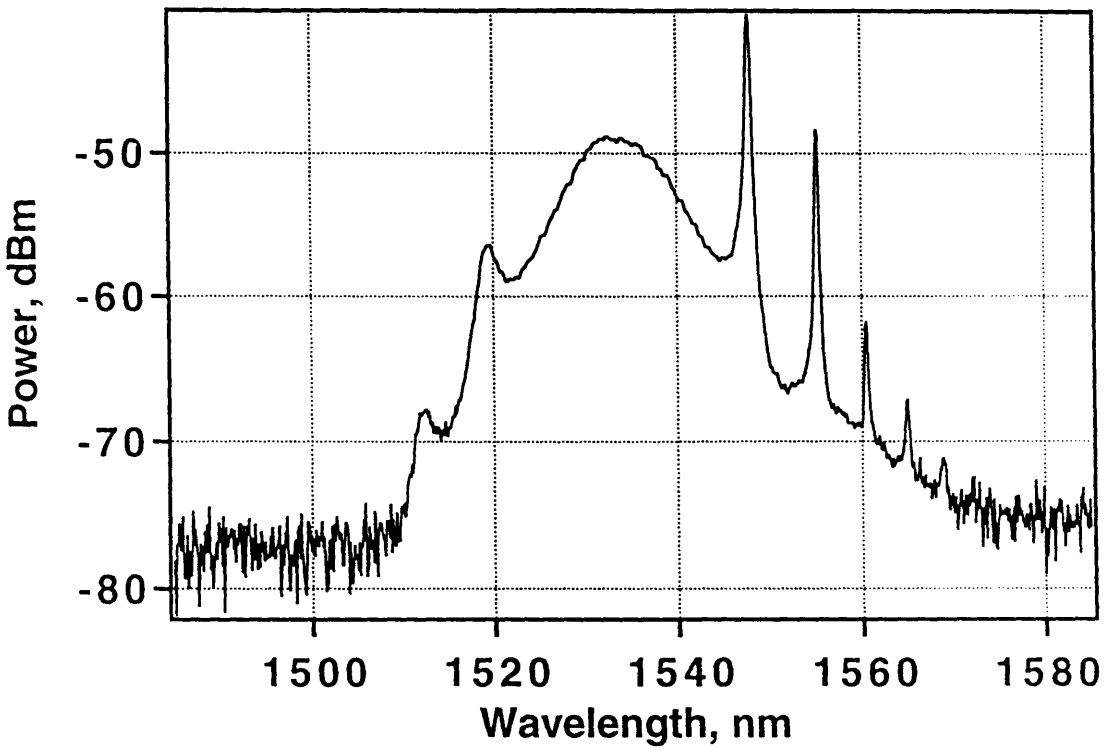

Figure 4-2: The optical spectrum of the soliton laser output

result. Figure 4-3 shows the 0th harmonic of the laser detector current's power spectrum. This harmonic has no timing jitter. The structure that occupies the frequency range of [-400 Hz, 400 Hz] is identified to be the amplitude fluctuation due to components of the pump noise that are slow compared with the erbium ion's relaxation time. The noise at very low frequencies is buried under the signal, and is ignored for now. Through the Kramers-Kronig relation, amplitude fluctuations cause a timing jitter which can be calcu-

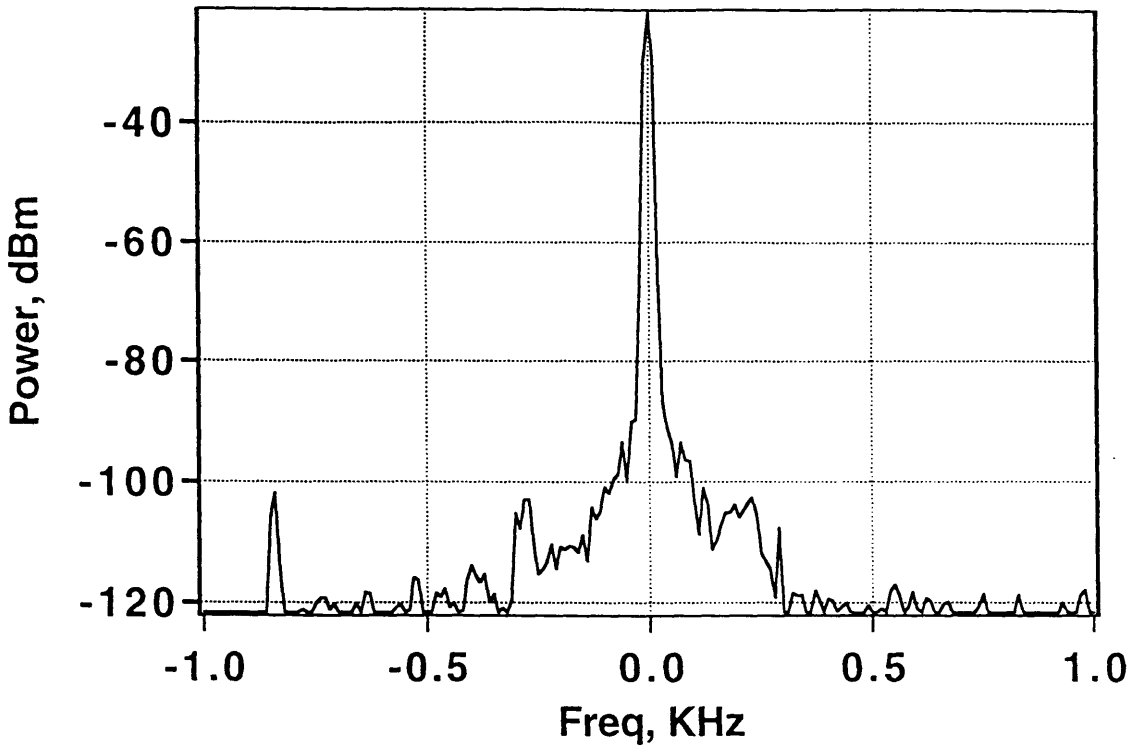

Figure 4.3: Harmonic 0 of the soliton RF spectrum

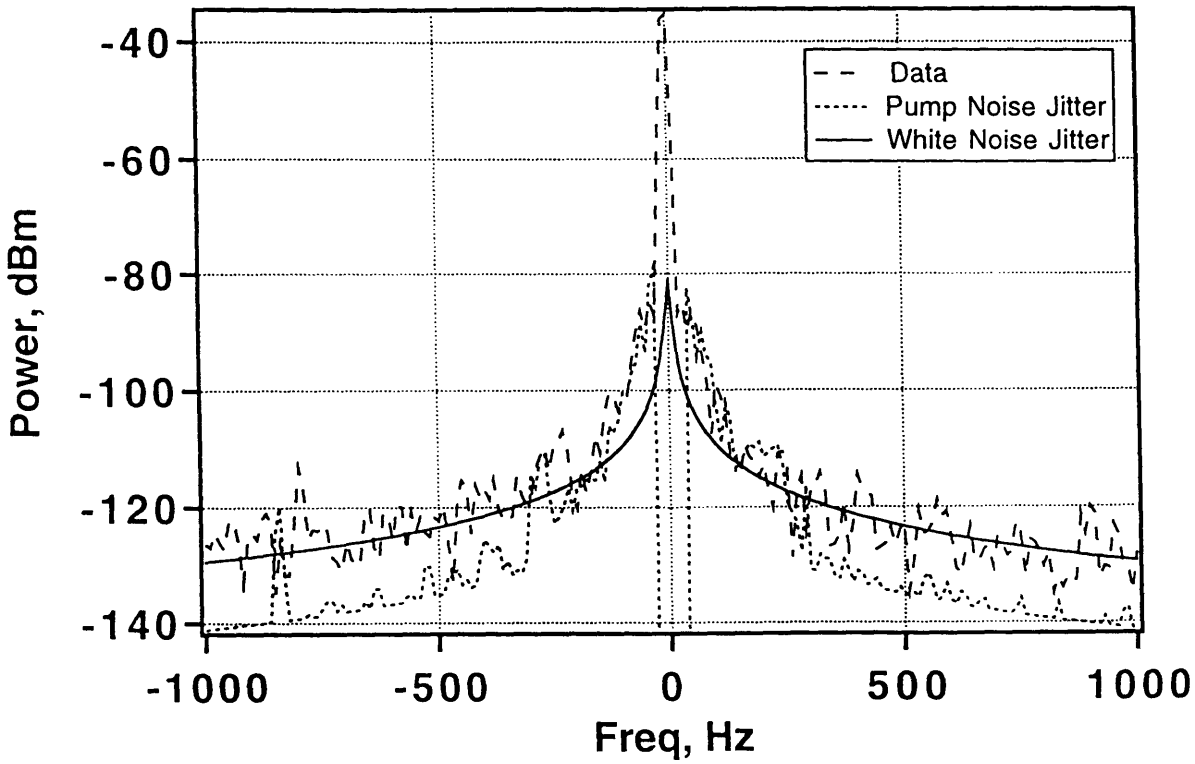

Figure 4.4: Timing jitter structures due to pump noise and due to white noise for harmonic 35

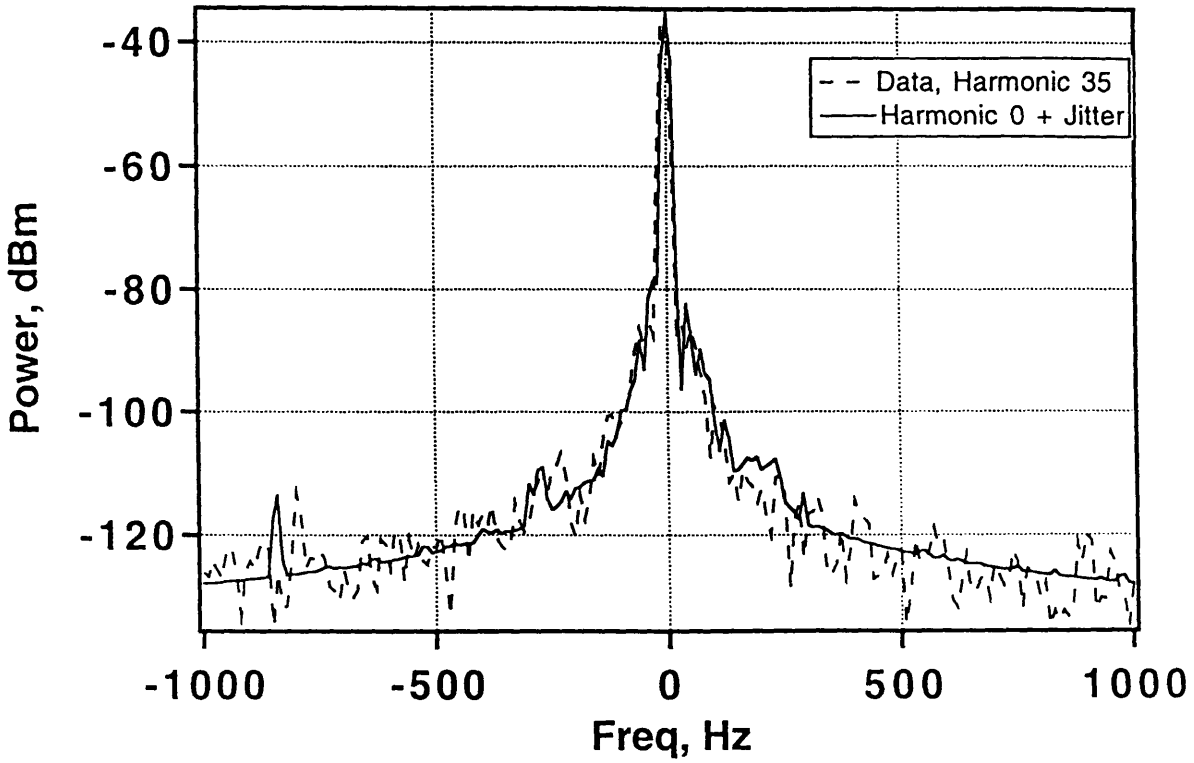

Figure 4.5: Fitting for harmonic 35

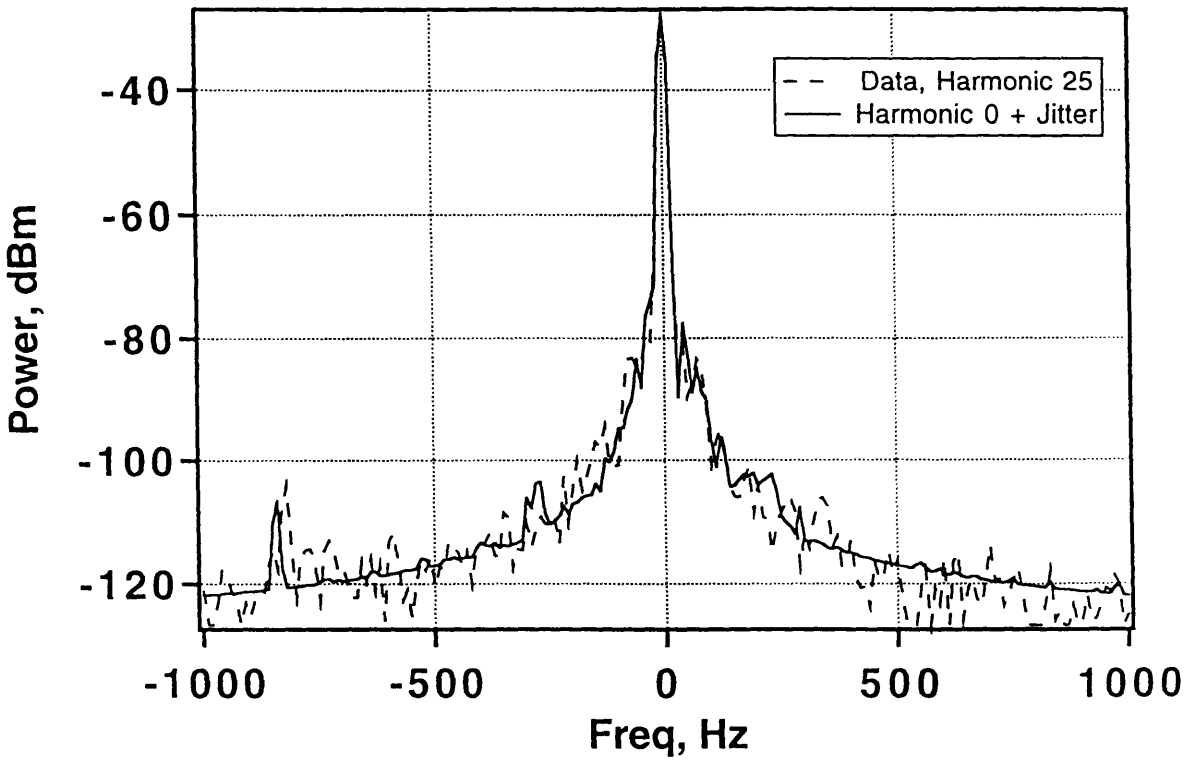

Figure 4.6: Fitting for harmonic 25

lated using (3.24). Because the pump noise spectrum is not sharply peaked, we are justified to use an infinite integration time when calculating the timing jitter. The symmetry in the timing jitter spectra(Figures 4-4-4-6) shows that the cross-correlation between Δw and Δt is negligible. Using (3.24) and (3.28) but ignoring the cross-correlation terms, we have computed the jitter due to this amplitude noise and find that an additional white noise source must be present in order to explain the jitter structure at frequencies greater than 400 Hz(Figure 4-4). To quantify this white noise jitter, (3.32) and (3. 33) have been used to fit the experimental data at frequencies greater than 400 Hz, with τp and D_{pp} as fitting parameters. τp is found to be 0.17 μs.

By adding both pump noise jitter and white noise jitter structures to Harmonic 0, one can predict the higher harmonics. Figure 4-5 overlays the experimentally measured Harmonic 35(dashed line), with the predicted Harmonic 35(solid line). The agreement is excellent. Figures 4-6 shows the same excellent agreement for Harmonic 25.

Equation (3.35) is used to quantify the timing jitter. The r.m.s value of the timing jitter due to white noise and the one due to pump noise are calculated separately. Taking into account the resolution bandwidth of the RF, we use the following relationship to fit the jitter data:

$$\frac{\int P_J(\Omega)\, d\Omega}{\Delta\Omega_{res} P_o} = (2\pi k)^2 \left(\frac{\Delta t}{T}\right)^2 \qquad (4.1)$$

where $P_J(\Omega)$ is the noise spectrum, and P_o is the peak power of the signal.

From the fitting, the jitter due to white noise is 27 ppm of the round trip time(0.65 ps), as shown in Figure 4-7. No method is available to accurately extract the very low fre-

quency amplitude fluctuations which are buried under the signal. Because of its $1/\Omega^2$ dependence, timing jitter at these frequencies can have a significant effect. If zero amplitude fluctuation is assumed for Δw at these very low frequencies, the r.m.s. jitter is 25

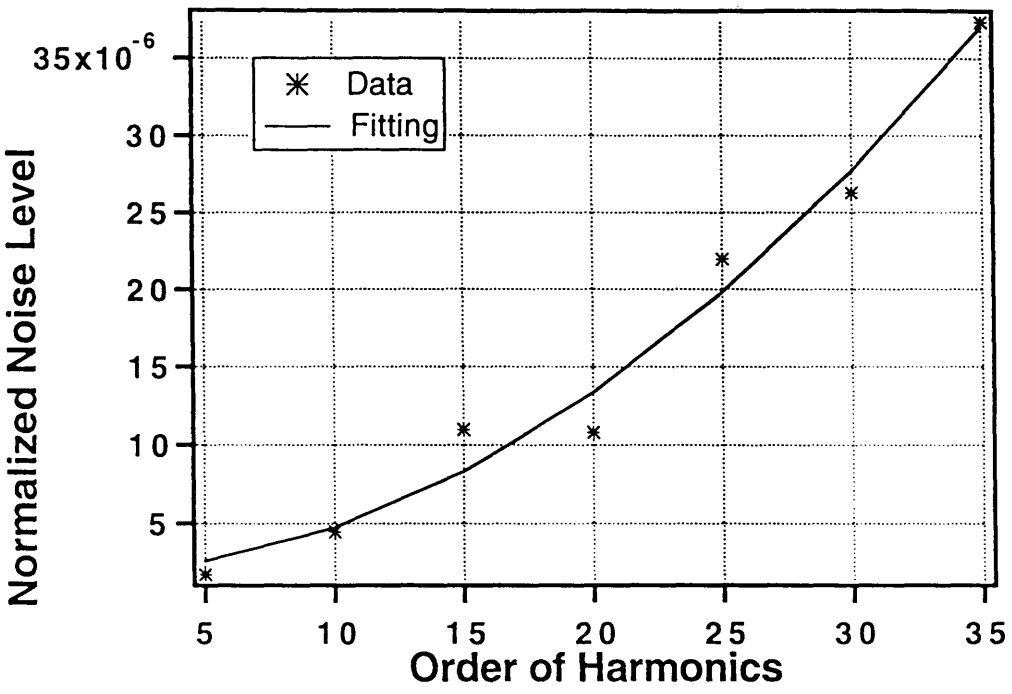

Figure 4-7: Timing jitter due to white noise, jitter=27 ppm

ppm of the round-trip time. The jitter is still low compared with those reported previously [13]-[19].

A similar analysis can be used to extract the amplitude noise.Two amplitude noise structures have been observed. One of them is the pump noise, as mentioned before. The noise contribution from this structure is about 0.05% of the average pulse energy. The other structure, as shown in Figure 4-8, spans a wider frequency range and is observed with a resolution bandwidth of 3 KHz. This structure contributes about 0.14% of the pulse

energy. If we assume that this structure has a white origin and do a fit using (3. 23), τ_w found to be 1 μs.

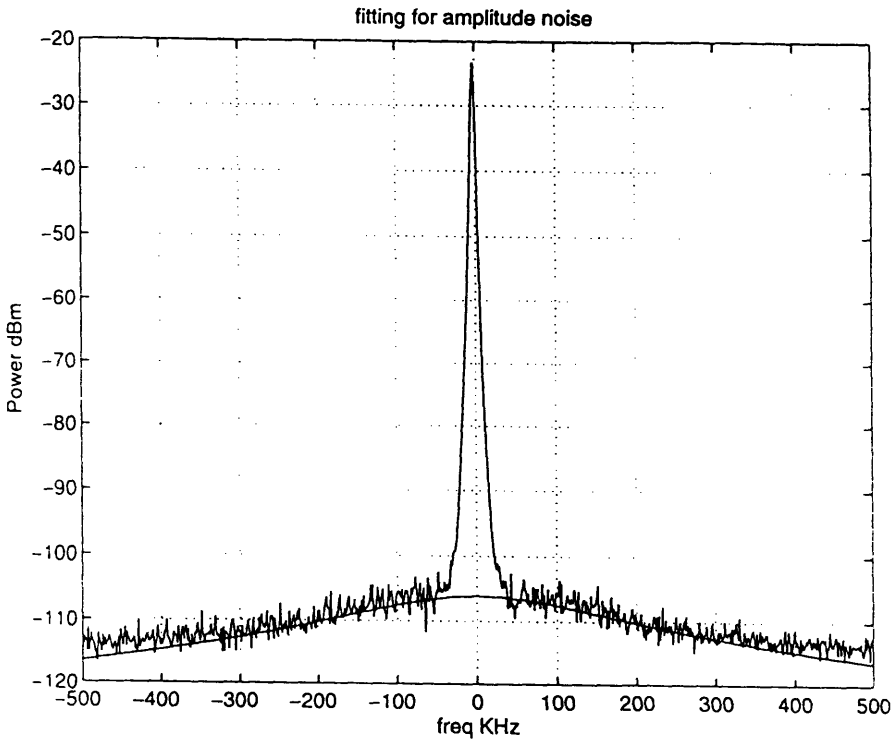

Figure 4-8: Energy fluctuation of the soliton laser

4.2.2 Comparison Between Theory and Experiments

The spontaneous emission noise(quantum noise) can be modelled by a white noise source with correlation [6], [35],[36]

$$<S_{qn}(T,t)\,S^{*}_{qn}(T',t')> = \theta\frac{2g}{T_R}h\nu\delta(T-T')\,\delta(t-t')\,. \qquad (4.2)$$

where θ is the enhancement factor due to incomplete inversion of the medium. The different components of this noise are

$$<S_{i,qn}(T)\,S_{h,qn}(T')> = D_{i,qn}\delta_{i,h}\delta(T-T') \tag{4.3}$$

with diffusion constants:

$$D_{w,qn} = 4w_o\theta\frac{2g}{T_R}h\upsilon \tag{4.4}$$

$$D_{\theta,qn} = \frac{4}{3w_o}\left(1+\frac{\pi^2}{12}\right)\theta\frac{2g}{T_R}h\upsilon \tag{4.5}$$

$$D_{p,qn} = \frac{2}{3w_o\tau^2}\theta\frac{2g}{T_R}h\upsilon \tag{4.6}$$

$$D_{t,qn} = \frac{\pi^2\tau^2}{3w_0}\theta\frac{2g}{T_R}h\upsilon \tag{4.7}$$

Noise induced by spontaneous emission can be calculated by solving Equations (3.22)-(3. 25) using (4.2)- (4.5) as the noise sources.

An expression for the r.m.s value of the quantum limited timing jitter has been derived by Haus and Mecozzi. It is:

$$<|\Delta t(T+T_o) - \Delta t(T_o)^2|> = \frac{4D^2}{T_R^2}\,D_{p,qn}\tau_p^3\left(\frac{T}{\tau_p} - 1 + e^{-T/\tau_p}\right) \tag{4.8}$$

where $D_{p,qn}$ is given by (4. 6), and T is the integration time(=0.1 second in our experiment).

In our case $T >> \tau p$, so (4. 8) becomes

$$<|\Delta t(T+T_o) - \Delta t(T_o)^2|> = \frac{4D^2}{T_R^2}\,D_{p,qn}\tau_p^2 T \tag{4.9}$$

Here τ=170 fs, D=-0.0768ps^2, g=0.79, w_o=175pJ, round trip time T_R= 24 ns and τp=0.17

μs from fitting of the experimental data. At 980 nm, θ is greater than two. If θ=2 is used, the r.m.s value of the quantum-limited timing jitter is 20ppm of the round-trip time. If θ=2.6 is used, then the jitter is 27 ppm, which is identical to the experimental value. Good agreement has been reached when quantum noise is plotted against experimental data(Figure 4-9). Thus, the timing jitter with a white noise origin is induced by spontaneous emission fluctuations.

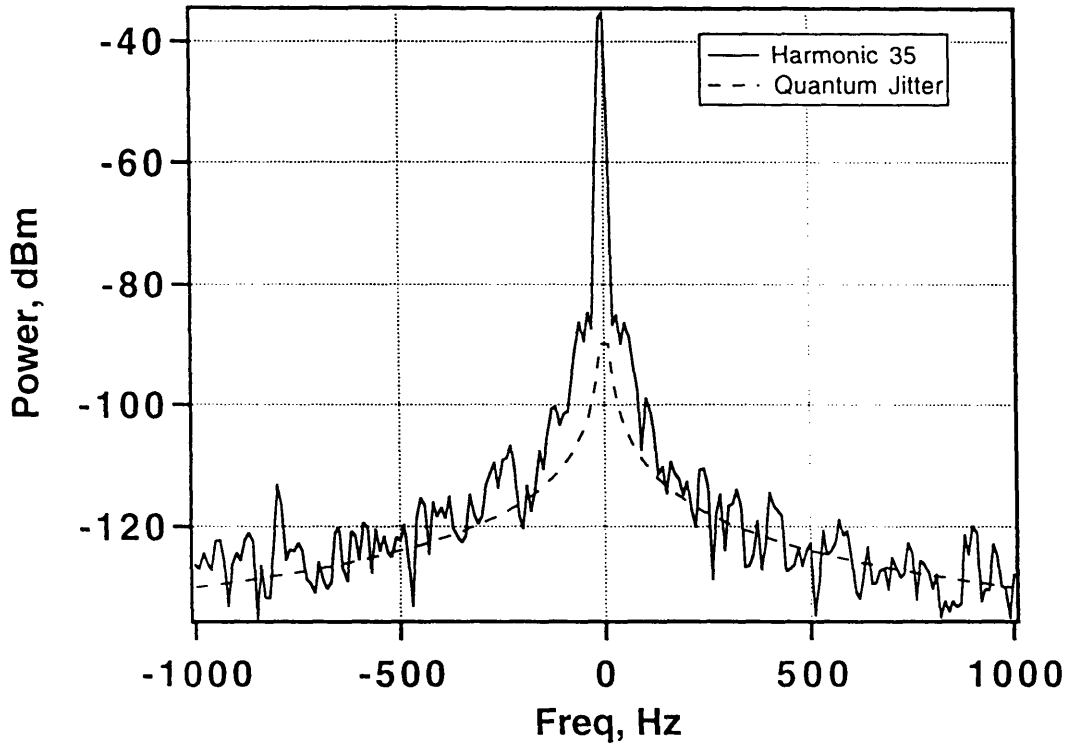

Figure 4-9: Theoretically predicted quantum jitter and experimental data for harmonic 35

Equation (4. 9) also indicates that the r.m.s jitter has the form of a random walk, i.e. the jitter value increases linear with T. We have also measured the jitter using a measurement time of 0.025 seconds. The resulting Δt/T induced by the white noise is found to be 11ppm. Thus, consistent measurement time is necessary in order to compare the measured

jitter values of different laser systems. The measured and calculated jitters are summarized in the Table 4-1:

Table 1: Summary of different timing jitter values for the soliton laser

T_{meas} (second)	Measured White Noise Jitter(ppm)	Calculated Quantum Jitter/ θ=2 (ppm)	Pump Noise Jitter(ppm)
0.1	27	20	>25
0.025	11	10	

Similarly, one can take the Fourier Transform of (3. 23), and derive the autocovariance of the energy fluctuation:

$$<\Delta w(T+T_o)\,\Delta w(T_o)>=\frac{\tau_w}{2}D_{w,w}e^{-|T|/\tau_w} \qquad (4.\ 10)$$

where $D_{w,w}$ is given in (4. 4). The r.m.s. value of energy fluctuation is $\frac{\sqrt{\tau_w D_{ww}/2}}{w_o}$, and is found to be 0.04%. This value is three times smaller than the one calculated in the previous section(0.14%). The presence of other noises, such the gain fluctuation, might be able to account for the discrepancies.

4.3 Noise of the Stretched Pulse Laser[47]

Figure 4-10 shows a schematic of the laser in its "reverse operation". Output coupling is provided by three 3.3% output ports. The net dispersion of the laser is 0.009 ps^2. The cavity round trip time is 27.7 ns, and the average pulse power is 0.45 mW at port 2. By reversing the isolator and the order of the waveplates, one can operate the laser in its "forward" direction, an operation whose average pulse power at port 3 is 1.04 mW. The erbium fiber

is pumped by a master-oscillator/power amplifier (MOPA) diode operating at 980 nm. This pump is essential to achieve low noise performance.

Figure 4-11 shows an optical spectrum of the laser output in its forward regime. Figure 4-12 & Figure 4-13 show a set of spectra of the 1st and 35th harmonic produced by the laser operating in the forward direction. The white noise jitter is too small to be quantified exactly. Figures 4-14 and 4-15 show the 1st and 35th harmonic produced by laser operating in the reverse direction. The white noise jitter is 4 ppm of the round-trip time. Two energy fluctuation structures have been found for both operations. For the reverse operation, the narrow-band structure that spans 400 Hz is determined from the first harmonic, and is 0.16%(Figure 4-14). The one that spans 400 KHz gives a fluctuation of 0.05%(Figure 4-16). For the forward operation the energy fluctuations are 0.2% and 0.08%, respectively. By adjusting the polarization controllers, one can also bias the laser so that the jitter structure is more visible, as shown in Figure 4-17. In this case the jitter is 19 ppm. The sharp spikes, which are present in all the graphs, are spaced about 420 Hz apart, and could be due to an external vibrating source.

4.4 Comparison between the Soliton Laser Noise and the Stretched Pulse laser Noise

Figure 4-17 shows that, unlike the noise structures for the soliton laser, the structure for the stretched pulse laser is asymmetric. Because the amplitude noise structure has a sharp cutoff at low frequencies, the asymmetry of the structure shown cannot be due to the energy-timing cross-correlation in (3. 28). One must conclude that the timing jitter structure of a stretched pulse laser can be made asymmetric. This feature is expected since the expansion functions (3. 39)-(3. 43) and their adjoints (3. 44)-(3. 49) are not all pair-wise orthogonal. In particular, f_p and f_t, the expansion functions for the frequency deviation and the timing jitter, are both first order gaussians. So the driving noise sources S_p and S_t are

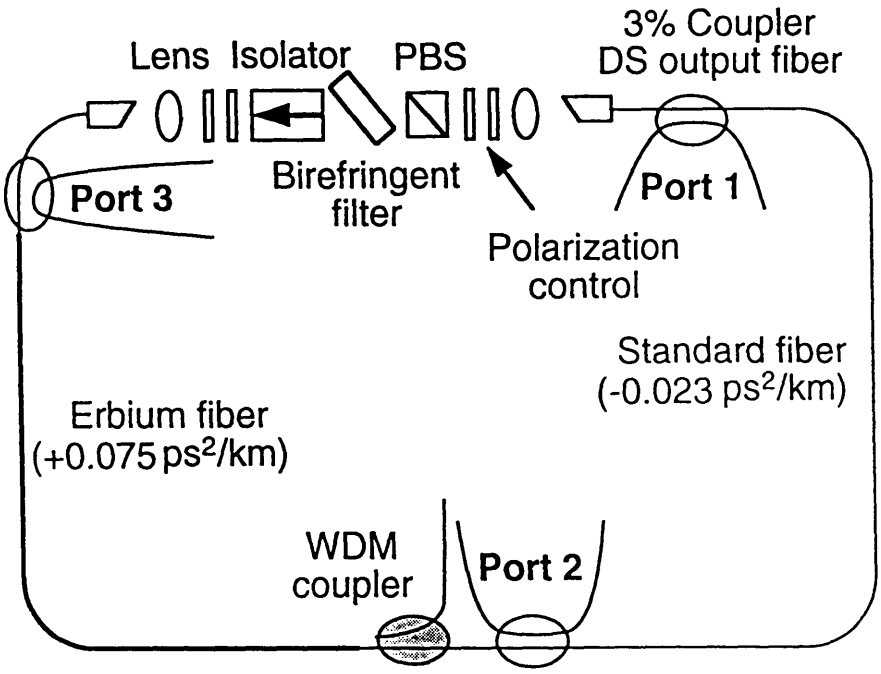

Figure 4.10: The stretched pulse laser used for the noise measurement

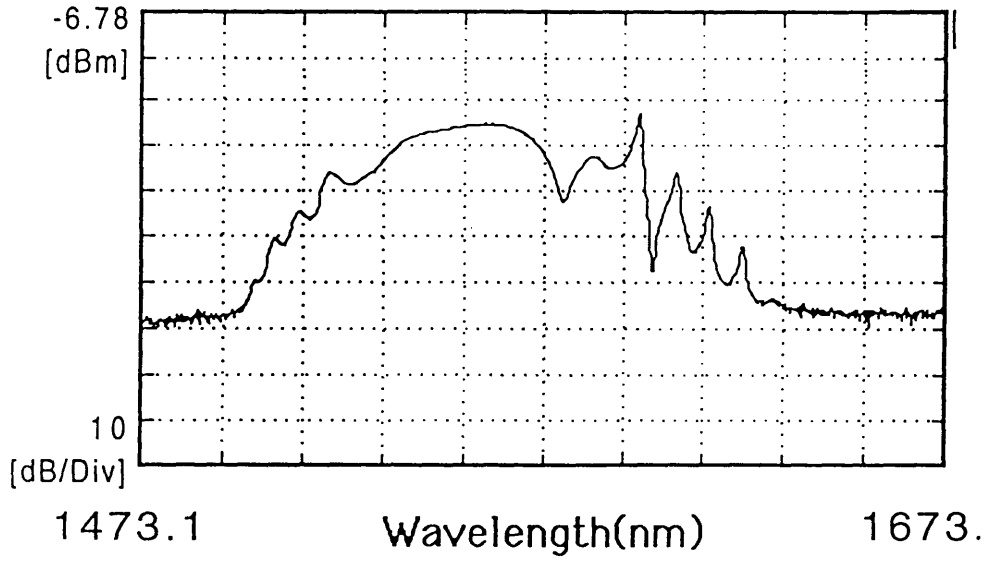

Figure 4.11: Optical spectrum of the stretched pulse laser in the forward regime

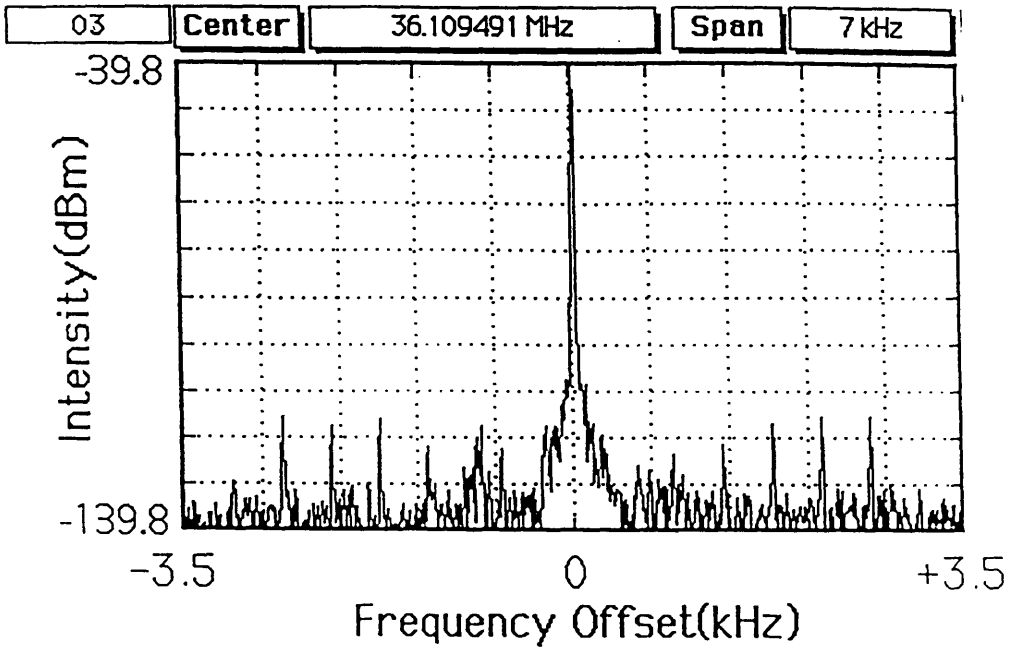

Figure 4.12: Harmonic 0 of the RF spectrum for the stretched pulse laser operating in the forward regime

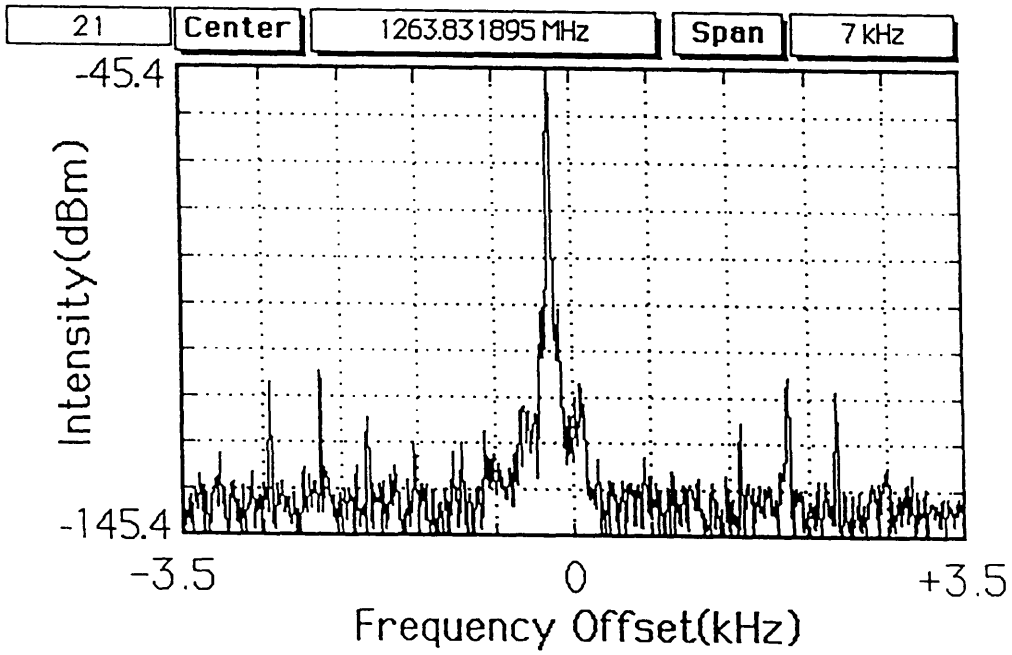

Figure 4.13: Harmonic 35 of the RF spectrum for the stretched pulse laser operating in the forward regime

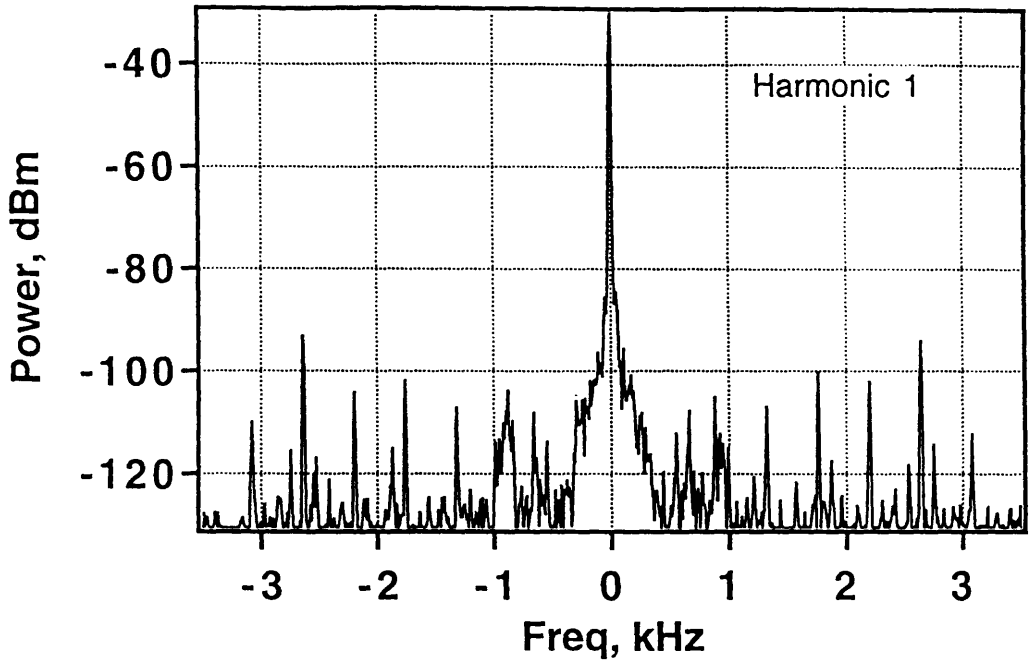

Figure 4.14: Harmonic 0 of the RF spectrum for the stretched pulse laser operating in the reverse regime

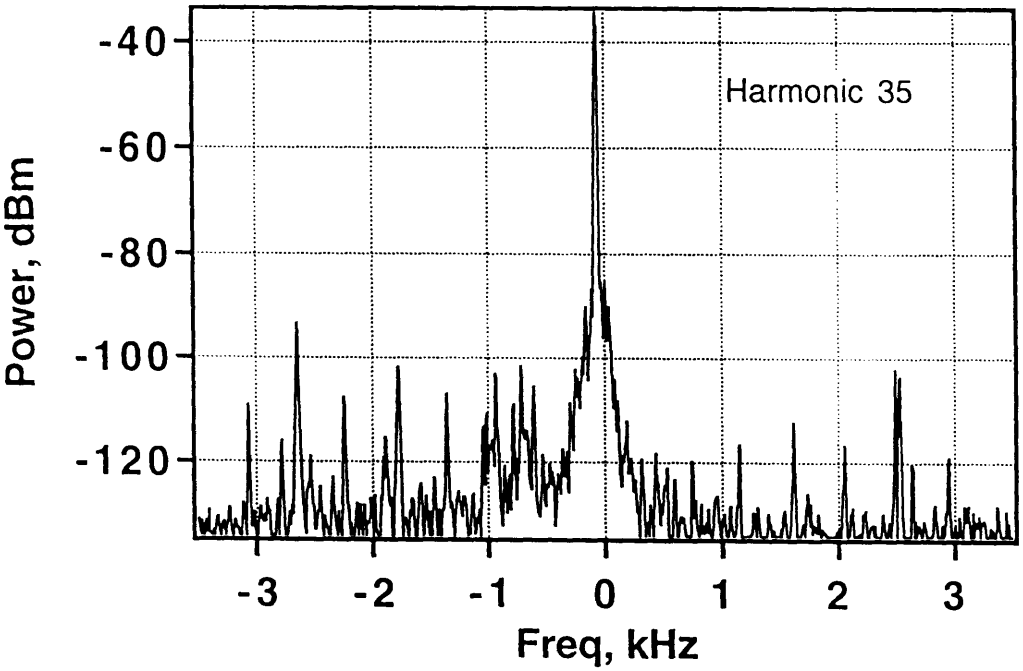

Figure 4.15: Harmonic 35 of the RF spectrum for the stretched pulse laser operating in the reverse regime

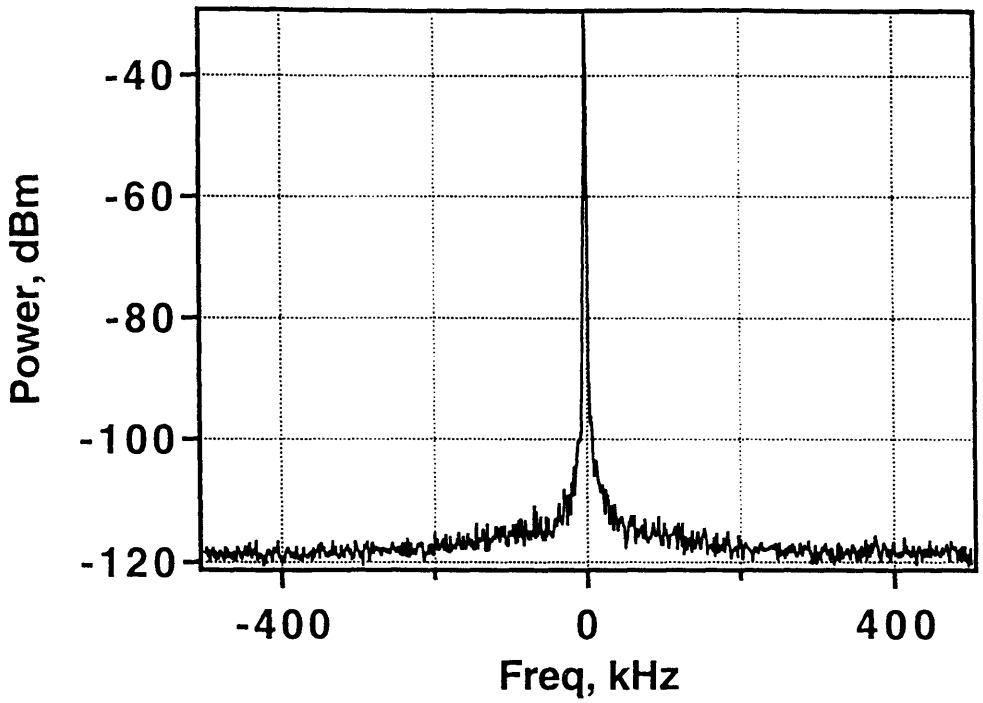

Figure 4.16: Energy fluctuation for the stretched pulse laser operating in the reverse regime

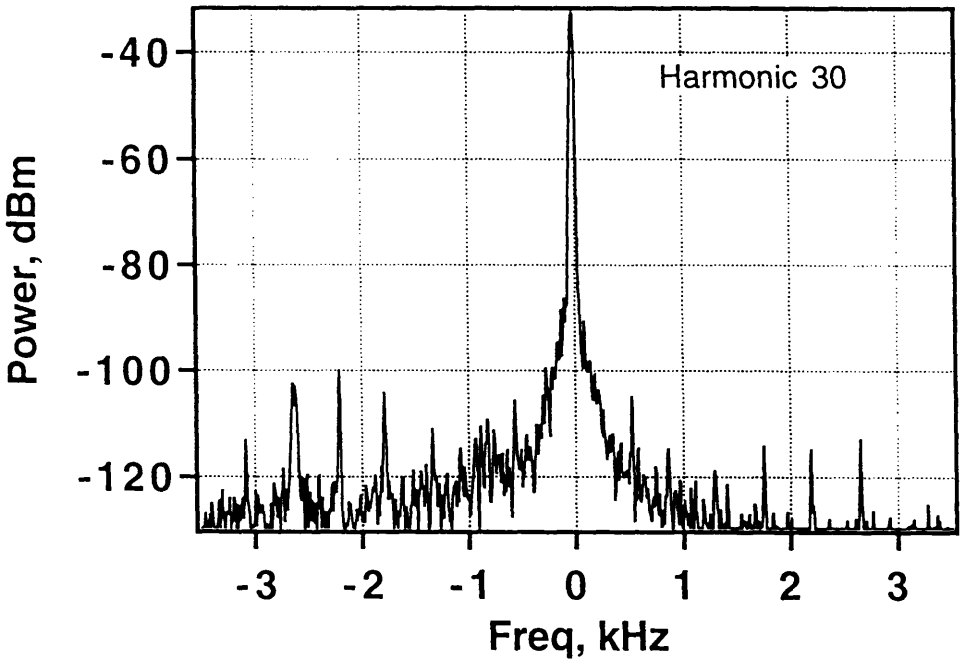

Figure 4.17: Inherent asymmetry of the timing jitter structure

correlated. Since Δp affects Δt by (3. 53), the correlation $<S_p(\Omega)S_t^*(\Omega)>$ contributes to the timing jitter psd, and causes the asymmetry.

Another feature of the stretched pulse output is its low timing jitter, comparing to the soliton laser. For the forward operation the jitter can be made negligibly small(Figure 4-13), and for the reverse operation the jitter is as low as 4 ppm(Figure 4-15). This can again be explained by the noise theory. The two timing jitter noise sources: GVD effect and filtering effect, both have smaller magnitudes in the case of the stretched pulse laser. The GVD of the tested stretched pulse laser is an order of magnitude smaller than the GVD of the soliton laser. Furthermore, the GVD of the stretched pulse laser can be zero, thus eliminating the effects from this noise origin altogether. The filtering action also has a smaller impact on the stretched pulse laser than on the soliton laser, even though the output from the former is slightly chirped. This is because the filter bandwidth of the former is much wider than that of the latter. The impact of filtering on the timing jitter is inversely proportional to the filter bandwidth.

Finally, the stretched pulse laser even has smaller amplitude fluctuations as well. This is very surprising: the laser undergoes large changes per round trip, and must be more susceptible to external perturbations than the soliton laser. This surprise can be explained if one assumes that the dominant cause of the amplitude noise is the amplified spontaneous emission. The stretched pulse laser has higher output power, thus more photons. So the effects due to one photon is not as large as in the soliton case. Indeed, the very low frequency structure due to the pump noise is larger than the one in the soliton case even though the MOPA is quieter than the pump diodes. This is an indication that if the magnitudes of the noise sources relative to the pulse power are comparable, the stretched pulse laser output will experience more amplitude fluctuation than the soliton laser output.

Chapter 5

Summary and Future Work

5.1 Summary

In this thesis we have investigated, both theoretically and experimentally, the noise characteristics of APM lasers, especially those of the soliton laser and the stretched pulse laser, In chapter 2 we have reviewed the theory of APM in fiber lasers. APM is first qualitatively described. We then reviewed the master equations of the soliton laser and the stretched pulse laser. In chapter 3 we have reviewed the noise theory of modelocked lasers. We first presented the background information in stochastic processes that is necessary to understand the random nature of the noise. D. von der Linde's phenomenological approach is then presented. The Haus-Mecozzi noise theory for the soliton laser and the noise theory for the stretched pulse laser are described. Both are perturbational approaches, and both provided physical insights into the noise mechanisms for these lasers. Chapter 4 describes the experimental results and analysis. The experimental results confirm the theoretical predictions. Comparison between the two lasers revealed striking similarities in terms of their noise characteristics.

5.2 Future Work

A disadvantage of extracting the noise structures from the power spectrum is that frequency fluctuation and phase noise are lost. One way to detect these types of noises is to use a cascade of Fabry-Perot interferometers to isolate the 0th harmonic of the pulse spectrum. The fluctuations in phase and frequency can then be characterized [11].

Another drawback of noise characterization via the power spectrum is the cutoff frequency of the fast photodiode detector and the RF spectrum analyzer, a cutoff which limits the use of the power spectrum method to low repetition rate lasers. The cutoff of the fast detector is usually around 1 GHz, but could be made as high as 40GHz, though the signal to noise ratio (SNR) at high frequencies is not good enough to study lasers with noise characteristics comparable to the ones presented in this thesis. Some RF spectrum analyzers have ranges up to 50 GHz, though the resolution bandwidth(RBW) at higher frequencies is not nearly as good as the one for frequencies less than 5 GHz. The combination of poor SNR of the detector and limited RBW of the spectrum analyzer make applying the present methodology to the high repetition rate laser impossible.

An example of a high repetition rate laser is the Asynchronously Modelocked laser [48], which can operate around 1 GHz. In this case only lower harmonics can be detected accurately, and the k^2 frequency dependence of the timing jitter structure may not be discerned. A possible solution is first demonstrated by Mollenaur [49], [50] to measure the Gordon-Haus jitter[35] in long-haul telecommunications. The power spectrum of an ideal pulse train has an envelope determined only by the pulse duration and the pulse shape. Jitter in the time domain leads to multiplication by a random phase factor in the frequency domain. The time average of this random phase pattern leads to a reduction in this envelope. Assuming that the jitter has a gaussian distribution, the reduction is also a gaussian as a function of frequency. The rms value of the jitter can then be calculated by comparing the measured envelope with the ideal envelope. Because only the envelope is needed, the limitations imposed by the detector and the RF spectrum analyzer are not important.

However, for very high repetition rate systems such as self-regenerative modelocked laser [51] or time division multiplexing (TDM) [14], the repetition rate can be as

high as 100 GHz. Power spectrum cannot be used to characterize noise in these systems because only the first few harmonics can be measured.

Though frequency domain methods become impractical to extract the noise of the high-repetition rate laser sources, time domain methods can be used for such purpose. One method is to take the cross-correlation of two pulses that are spaced n pulses apart[55]. Such measurement usually results in an envelope with a fringe pattern underneath it. If the energy of the second pulse differs from the first pulse, and/or if the timing of the second pulse deviates from the round-trip time, there will be a shift in the fringe pattern underneath the envelope. A very noisy laser leads to a very big shift in the fringe pattern. Since there is no restoring force, the timing jitter of a passively modelocked laser is a random walk. So a sufficiently long delay between the two pulses will eventually produce a detectable shift in the fringe pattern. This method should be practical for very high repetition rate lasers since the coherence times of these lasers may be long enough comparing to their repetition rates so that cross-correlation is possible.

The next challenge will be to improve the noise performance of these lasers, and to use these low noise sources in different applications. Squeezing experiments, for example, can definitely benefit from these sources. Hopefully this thesis will prove to be useful towards these purposes.

Bibliography

[1] A. Yariv, *Optical Electronics*, 4th ed., New York: Sauders College Publishing, 1991.

[2] H. A. Haus, *Waves and Fields in Optoelectronics*, New Jersey: Prentice Hall, 1984.

[3] H. A. Haus, "Theory of modelocking with a fast saturable absorber," *J. Appl. Phys.*, vol 46, pp. 3049-3058, 1975.

[4] H. A. Haus, J. G. Fujimoto, and E. P. Ippen, "Structures for additive pulse mode locking," *J. Opt. Soc. Am. B*, vol 8, p.2068, 1991.

[5] E. P. Ippen, H. A. Haus, and L. Y. Liu, "Additive pulse mode locking," *J. Opt. Soc. Am. B*, vol 6, p. 1736, 1989.

[6] D. von der Linde, "Characterization of the noise in continuously operating modelocked lasers," *Appl. Phys. B*, vol. 39, p. 201, 1986.

[7] A. Finch, X. Zhu, P. N. Kean, and W. Sibbett, "Noise characterization of modelocked lasers," *Appl. Phys. B*, vol 39, p.201, 1986.

[8] U. Keller, C.E. Soccolich, G. Sucha, M. N. Islam, and M. Wegener, "Noise characterization of femtosecond color-center lasers," *Opt. Lett.*, vol. 15, p.974, 1990.

[9] G. T. Harvey, M. S. Heutmaker, P. R. Smitth, M. C. Nuss, U. Keller, and J. A. Valdmanis, "Timing jitter and pump-induced amplitude modulation in the colliding pulse modelocked(CPM) laser," *IEEE J. Quantum Electron.*, vol. 27, p.295, 1991.

[10] S. B. Darack, D. R. Dykaar, and G. T. Harvey, "Timing-jitter stabilization of a colliding-pulse mode-locked laser by active control of the cavity length," *Opt. Lett.*, vol. 16, p. 1677, 1991.

[11] H. A. Haus and A. Mecozzi, "Noise of mode-locked lasers," *IEEE J. Quantum Electron.*, vol 29, p. 983, 1993.

[12] J. A. Izatt, M. R. Hee, D. Huang, J. G. Fujimoto, E. A. Swanson, C. P. Lin, J. S. Schuman, and C. A. Puliafito, "Optical coherence tomography for medical diagnostics," in Medical Optical Tomography: Functional Imaging and Monitoring, vol. IS11, pp.450-472, SPIE Institutes: Institutes for Advanced Optical Technologies, 1993.

[13] M. R. Hee, J. A. Izatt, J. Jacobson, E. A. Swanson, and J. G. Fujimoto, "Time-gated imaging with femtosecond transillumination optical coherence tomography," in Photon Migration and Imaging in Random Media and Tissues(B. Chance, ed.), vol. Proc. SPIE 1888, SPIE, 1993.

[14] H. Takara, S. Kawanishi, T. Morioka, K. Mori, and M. Saruwatari, "0.6 ps resolution, 100 gbp/s optical wavefom measurement by optical sampling using supercontinuum subpicosecond pulses," in *CLEO Postdeadline Papers*, (Anaheim, CA), May 8-13 1994. Paper CPD10.

[15] C. R. Doerr, K. Tamura, M. Shirasaki, H. A. Haus, and E. P. Ippen, "Orthogonal polarization fiber optic gyroscope with improved stability," *Appl. Opt.*, 1994. accepted for publication.

[16] K. Bergman and H. A. Haus, "Squeezing in fibers with optical pulses," *Opt. Lett.*, vol. 16, pp. 663-665, 1991.

[17] M. Shirasaki, and H. A. Haus, "Squeezing of pulses in a nonlinear interferometer," *J.*

Opt. Soc. Am. B, vol. 7, pp. 30-34, 1990.

[18] L. Boivin, *Squeezing in fiber lasers*, PhD thesis, MIT, 1995.

[19] C. R. Doerr, *Steps toward a noiseless fiber optic gyroscope*. Ph. D. thesis, MIT, 1994.

[20] L. F. Mollenauer and R. H. Stolen, "The soliton laser," *Opt. Lett.*, vol. 9, pp. 13-15, 1984.

[21] H. A. Haus, E. P. Ippen, and K. Tamura, "Additive-pulse modelocking in fiber lasers," *IEEE J. Quantum Electron.*, vol 30, p.200, 1994.

[22] H. A. Haus, J. G. Fujimoto, and E. P. Ippen, "Analytic theory of additive pulse and kerr lens mode locking," *IEEE J. Quantum Electron.*, vol 28, p. 2086, 1992.

[23] M. Hofer, M. E. Fermann, F. Haberl, M. H. Ober, and A. J. Schmidt, "Mode locking with cross-phase and self-phase modulation," *Opt. Lett.*, vol. 16, pp. 502-504, 1991.

[24] K. R. Tamura, *Additive pulse mode-locked erbium-doped fiber lasers*. PhD thesis, MIT, 1994.

[25] J. Mark, L. Y. Liu, K. L. Hall, H. A. Haus, and E. P. Ippen, "femtosecond pulse generation in a laser with a nonlinear external resonator," *Opt. Lett.*, vol. 14, pp. 48-50, 1989.

[26] E. P. Ippen, L. Y. Liu, and H. A. Haus, "Self-starting condition for additive-pulse modelocking lasers," *Opt. Lett.*, vol. 15, pp.183-185, 1990.

[27] H. A. Haus and E. P. Ippen, "Self-starting of passively mode-lockd lasers," *Opt. Lett.*, vol. 16, pp. 1331-1333, 1991.

[28] K. Tamura, H.A. Haus, and E. P. Ippen, "Self-starting Additive Pulse Mode-Locked Erbium fiber ring laser," *Electron. Lett.*, vol 28, p. 2226, 1992.

[29] H. A. Haus, and W. S. Wong, "Solitons in Optical Communications", submitted to *Reviews of Modern Physics*.

[30] K. Tamura, E. P. Ippen, and H. A. Haus, "Pulse dynamics in stretched-pulse fiber lasers," *Appl. Phys. Lett.*, vol 67, pp. 158-160, 1995.

[31] K. Tamura, E. P. Ippen, H. A. Haus, and L. E. Nelson, "77-fs pulse generation from a stretched-pulse mode-locked all-fiber ring laser," *Opt. Lett.*, vol. 18, pp. 1080-1082, 1993.

[32] H. A. Haus and S. Namiki, "Noise Analysis of stretched pulse fiber laser: Quantum Electronics and Femtosecond Optics Memo 70," tech. rep., MIT, 1995."

[33] A. Willsky, G. W. Wornell, J. Shapiro, *6.432 course Notes*, MIT, 1995.

[34] J. N. Walpole, E. S. Kintzen, S. R. Chinn, C. A. Wong, and L. J. Missaggia, "High-power strained-layer InGaAs/AlGaAs tapered travelling wave amplifier," *Appl. Phys. Lett.*, vol 70, pp.740-742, 1992.

[35] J. P. Gordon and H. A. Haus, "Random walk of coherently amplified solitons in optical fiber transmission," *Opt. Lett.*, vol. 11, p. 665, 1986.

[36] H. A. Haus, "Quantum noise in a soliton like repeater system," *J. Opt. Soc. Am. B*, vol. 8, p. 1122,1991.

[37] D. E. Spence, J. M. Dudley, K. Lamb, W. E. Sleat, and W. Sibbett, "Nearly quantum-limited timing jitter in a self-mode-locked Ti:sapphire laser," *Opt. Lett.*, vol 19, p. 481, 1994.

[38] M. L. Dennis and I. N. Duling III, "Experimental study of sideband generation in femtosecond fiber lasers," *IEEE J. Quantum Electron.*, vol 30, p. 1469, 1994.

[39] J. P. Gordon, "Dispersive perturbations of solitons of the nonlinear Schrodinger equation," *J. Opt. Soc. Am. B*, vol 9, p. 91, 1992.

[40] D. E. Spence, J. M. Evans, W. E. Sleat, and W. Sibbett, "Regeneratively initiated self-mode-locked Ti:Sapphire laser," *Opt. Lett.*, vol 16, p. 1762, 1991.

[41] D. R. Walker, D. W. Crust, W. E. Sleat, and W. Sibbett, "Reduction of phase noise in passively mode-locked lasers," *IEEE J. Quantum Electron.*, vol. 28, p. 289, 1992.

[42] J. Son, J. V. Rudd, and J. F. Whitaker, "Noise characterization of a self-mode-locked Ti:Sapphire laser," *Opt. Lett.*, vol 17, p. 733, 1992.

[43] S. M. Kelly, "Characteristic sideband instability of periodically amplified average soliton," *Electron Lett.*, vol 28, p. 806, 1992.

[44] D. U. Noske, N. Pandit, and J. R. Taylor, "Source of spectral and temporal instability in soliton fiber lasers," *Opt. Lett.*, vol 17, p. 1515, 1992.

[45] S. Namiki, C. X. Yu, and H. A. Haus, "Observation of nearly quantum-limited timing jitter in an all-fiber ring laser," submitted to *J. Opt. Soc. Am. B.*

[46] S. Namiki, C. X. Yu, K. Tamura, H. A. Haus, and E. P. Ippen, , "Noise characteristics of a polarization additive pulse mode-locked fiber ring laser," *Laser and Electro-optical Society Annual Meeting*, 1995.

[47] C. X. Yu, S. Namiki, W. S. Wong, and H. A. Haus, "Noise performance of the stretched pulse ring laser," *Conference on Lasers and Electro-optics*, 1996.

[48] H. A. Haus, D. J. Jones, E. P. Ippen, and W. S. Wong, "Theory of soliton stability in asynchronous modelocking," to appear in *J. Lightwave Technol.*

[49] L. F. Mollenauer, M. J. Neubelt, S. G. Evangelides, J. P. Gordon, J. R. Simpson, and L. G. Cohen, "Experimental study of soliton transmission over more than 10,000 km in dispersion-shifted fiber," *Opt. Lett.*, vol 15, p.1203, 1990.

[50] L. F. Mollenauer and K. Smith, "Demonstration of soliton transmission over more than 4000 km in fiber with loss periodically compensaed by Raman gain," *Opt. Lett.*, vol 13, p.675, 1988.

[51] A. Takada and H. Miyazawa, "30 GHz picosecond pulse generation from actively

mode-locked erbium-doped fiber laser," *Elect. Lett.*, vol. 26, pp. 216-217, 1990.

[52] H. A. Haus, K. Tamura, L. E. Nelson, and E. P. Ippen, "Stretched-pulse additive mode-locking fiber ring laser: theory and experiemnt," *IEEE J. Quant. Electron.*, vol 31, pp.591-598, 1995.

[53] G. Lenz, K. Tamura, H. A. Haus, and E. P. Ippen, "All-solid-state femtosecond source at 1.55 um," *Opt. Lett.*, vol. 20, pp. 1289-1291, 1995.

[54] H. Stark and J. W. Woods, *Probability, Random Processes and Estimation for Engineers*, 2nd ed., New Jersey: Prentice Hall, 1994.

[55] The idea originated from Prof. Ippen.